REVIEWS

Journal of Semiconductors
(2021) 42, 041302
doi: 10.1088/1674-4926/42/4/041302

Photonic radio frequency channelizers based on Kerr optical micro-combs

Mengxi Tan[1], Xingyuan Xu[2], Jiayang Wu[1], Thach G. Nguyen[3], Sai T. Chu[4], Brent E. Little[5], Roberto Morandotti[6, 7], Arnan Mitchell[3], and David J. Moss[1, †]

[1]Optical Sciences Centre, Swinburne University of Technology, Hawthorn, VIC 3122, Australia

[2]Electro-Photonics Laboratory, Department of Electrical and Computer Systems Engineering, Monash University, VIC3800, Australia

[3]School of Engineering, RMIT University, Melbourne, VIC 3001, Australia

[4]Department of Physics, City University of Hong Kong, Hong Kong, China

[5]State Key Laboratory of Transient Optics and Photonics, Xi'an Institute of Optics and Precision Mechanics, Chinese Academy of Science, Xi'an 710119, China

[6]INRS -Énergie, Matériaux et Télécommunications, 1650 Boulevard Lionel-Boulet, Varennes, Québec, J3X 1S2, Canada

[7]Frontier Sciences, University of Electronic Science and Technology of China, Chengdu 610054, China

Abstract: We review recent work on broadband RF channelizers based on integrated optical frequency Kerr micro-combs combined with passive micro-ring resonator filters, with microcombs having channel spacings of 200 and 49 GHz. This approach to realizing RF channelizers offers reduced complexity, size, and potential cost for a wide range of applications to microwave signal detection.

Key words: microwave photonic; signal channelization; integrated optical frequency comb

Citation: M X Tan, X Y Xu, J Y Wu, T G Nguyen, S T Chu, B E Little, R Morandotti, A Mitchell, and D J Moss, Photonic radio frequency channelizers based on Kerr optical micro-combs[J]. *J. Semicond.*, 2021, 42(4), 041302. http://doi.org/10.1088/1674-4926/42/4/041302

1. Introduction

Nonlinear optics as a means to achieve ultrafast all-optical signal processing has been extremely powerful, and has focused on photonic integrated circuit platforms based on highly nonlinear materials such as silicon[1–3]. The range of signal processing operations that can be performed with nonlinear optical techniques is very large, and includes optical logic[4], optical temporal demultiplexing at ultra-high bit rates from 160 Gigabits/s[5] to well over a terabit per second[6], optical performance monitoring based on slow light[7, 8], signal regeneration[9, 10], and many other functions[11–16]. Complementary metal oxide semiconductor (CMOS) compatible platforms are extremely important since they can exploit the extensive global infrastructure established to fabricate computer chips. Since all CMOS compatible material platforms are centrosymmetric, the 2nd order nonlinear response is zero and so nonlinear devices in these platforms have been based on the 3rd order nonlinear susceptibility that accounts for processes including optical third harmonic generation[11, 17–21] as well as the instantaneous intensity dependent refractive index termed the Kerr nonlinearity (n_2)[1, 2]. The efficiency of all-optical devices based on the Kerr nonlinearity depends on the waveguide nonlinear parameter (γ), and although silicon waveguides and nanowires have achieved extremely high nonlinear parameters (γ), they also display quite high nonlinear optical loss arising from indirect two-photon absorption (TPA) in the telecommunications wavelength region (near 1550 nm), since the indirect bandgap of silicon is only 1.17 eV which is much less than twice the photon energy at 1550 nm. Moreover, worse than the intrinsic TPA is the effect of the resulting generated free carriers[2] since the carrier recombination time in silicon can be very long (microseconds), enabling significant carrier densities (and hence loss) to build up. Even if the effect of these carriers can be minimized through the use of p–i–n junctions to sweep out the carriers and greatly reduce the effective carrier lifetime, the intrinsic material nonlinear figure of merit [FOM = $n_2/(\beta\lambda)$, where β is the TPA and λ the wavelength] of silicon is only 0.3 in the telecom band. This is too low to achieve high all-optical performance and is a fundamental property of silicon's band structure and therefore cannot be improved. While TPA can be turned around and actually used as a positive tool for some nonlinear functions[22–24], for most processes silicon's low FOM in the telecom band poses a significant limitation. This has been the motivation for research into alternative nonlinear optical platforms, such as chalcogenide glass[25–34], for example. However, although many of these platforms offer significant advantages, most of them are not CMOS compatible, which ultimately is a fundamental consideration to achieve widespread and efficient manufacturing.

New CMOS compatible platforms for nonlinear optics were introduced in 2007/8 that exhibit negligible TPA in the 1550 nm wavelength regime. These include silicon nitride[35, 36] and high-index doped silica glass, trade-named Hydex[37–47]. In addition to having negligible nonlinear absorp-

Correspondence to: D J Moss, dmoss@swin.edu.au
Received 8 FEBRUARY 2021.

tion even up to many Gigawatts of power, these platforms have a moderate Kerr nonlinearity, resulting in an extremely high nonlinear FOM with a nonlinear parameter (γ) that is high enough to realize significant parametric gain. Following the first report of a micro-resonator based optical frequency comb source driven by the Kerr nonlinearity in 2007[48], the first fully integrated optical parametric oscillators based on micro-ring resonators (MRRs) were reported in 2010[36, 37] in these new CMOS compatible platforms of SiN and Hydex. Since 2010 the field of integrated micro-combs, or Kerr combs has become one of the largest and most successful fields in optics and photonics[47]. They are new and powerful tools to accomplish many new functions on an integrated chip, due to their very high coherence, while also offering flexible control of their wavelength spacing. Optical micro-combs are produced via optical parametric oscillation driven by modulational instability, or parametric gain, in integrated ring resonators. This offers huge advantages over more conventional approaches including discrete multiple laser wavelength sources. Many breakthroughs have been reported with Kerr micro-combs, from innovative mode-locked lasers[49–52] to quantum optical photonic chips[53–61], ultrahigh bandwidth optical fibre data transmission[62–64], optical neural networks[65–67], integrated optical frequency synthesizers[68] and more, and have been extensively reviewed[47, 69–76]. The success of these new CMOS platforms has motivated the search for even higher performing CMOS compatible platforms such as amorphous silicon[77] and silicon rich silicon nitride[78], searching for the ideal combination of low linear and nonlinear loss together with a high nonlinearity.

A significant application for microcombs has been in signal processing functions for telecommunications and RF/microwave systems, ranging from RF photonic applications to signal generation and processing for radar systems[79–128]. RF photonics is attractive because of its ultra-high bandwidth as well as low transmission loss and strong immunity to electromagnetic interference. There are different RF photonic approaches including methods that map the optical filter response onto the RF domain including devices based on stimulated Brillouin scattering[88–95], that have achieved high RF resolution — down to 32 MHz, as well as a stopband discrimination > 55 dB. A different but equally key approach to reconfigurable RF transfer functions for signal processing has been transversal filter methods[96–100]. These operate by generating progressively delayed and weighted replicas of an RF signal multicast onto many optical carriers, which are subsequently summed via photo-detection. Transverse filters can achieve a wide range of RF functions solely by varying the tap weights, and so this approach is very attractive for advanced dynamically adaptive RF filters. Discrete diode laser arrays[101] and fibre and integrated Bragg grating arrays and sampled gratings[103] have been used to generate the required taps. However, while offering advantages, these methods have increased complexity and footprint, limiting performance due to the limited number of wavelengths. Alternative methods such as electro-optic (EO) or acousto-optic (AO) combs[102, 104, 105], can help overcome this, but they require many high bandwidth modulators and high-frequency RF sources.

Kerr micro-combs[36, 37] have been very successful in their applications to RF systems, providing advantages over other methods of supplying multiple wavelengths for RF photonic systems. They have achieved extremely high bandwidth data communications as well as a wide range of microwave signal processing devices[107–128]. Their comb spacings can be much wider than electro-optic combs, and in many ways EO and micro combs are complementary. EO combs excel at finer spacings from 10's of megahertz to 10–20 GHz, while integrated micro-combs typically have much wider spacings from 10's of GHz to 100's of GHz and even THz. Larger comb spacings have much wider Nyquist zone for large RF bandwidth operation, whereas smaller spacings provide many more wavelengths or RF "taps", although at the expense of a smaller Nyquist zone. Micro-combs provide more wavelengths while still having a large free spectral range (FSR), all in a small footprint. For RF transversal filters the number of wavelengths determines the number of channels for RF true time delays and RF filters[85, 121]. Systems such as beamforming devices[112] can also be improved in quality factor and angular resolution. Other approaches to filtering include RF bandwidth scaling[125] that yields a particular bandwidth for each wavelength channel, where the total bandwidth (maximum RF signal bandwidth) will depend on the number of wavelengths which is dramatically increased with micro-combs.

Recently[121], we reviewed transversal filtering and bandwidth scaling methods based on Kerr micro-combs, as applied to RF and microwave spectral filters, followed by a review of temporal based signal processing[129]. In this paper, we review recent progress in microwave and RF photonic based channelizers based on Kerr micro-combs. We cover devices achieved with both widely spaced micro-combs with an FSR of 200 GHz[113] as well as results obtained with record low FSR micro-combs with a spacing of 49 GHz, operating via soliton crystals[122]. We highlight their potential and future possibilities, contrasting the different methods and use of the differently spaced micro-combs. While 200 GHz Kerr micro-combs have been successful for RF channelizers, achieving high levels of performance, high versatility and dynamic reconfigurability, their large comb spacing limited the number of channels as well as the RF bandwidth that can be achieved without the use of thermal tuning. This is an important consideration because RF channelizers need many components such as optical amplifiers and spectral shapers that are only available at telecom wavelengths (1530–1620 nm). The limitation in the number of channels has restricted the overall RF bandwidth, frequency resolution, and dynamic reconfigurability of micro-comb based RF channelizers. To overcome this, we focused on RF channelizers based on record low FSR combs, with a spacing of 49 GHz, in order to achieve over 90 channels in the C-band[122]. This represents the highest value for any micro-comb based RF channelizer. Our results confirm the feasibility of achieving high performance reconfigurable transversal RF filters for signal processing with reduced footprint, complexity, and cost. We first review the micro-combs used to realize the RF channelizers, followed by the results for 200 GHz microcomb based channelizers and finally by the 49 GHz soliton crystal based systems.

2. Integrated Kerr micro-combs

The formation of micro-combs is a complex process that arises from a combination of a high nonlinear parameter to-

gether with low nonlinear as well as linear loss, and finally from careful engineering of the dispersion. Micro-combs have been realized in a variety of material platforms[47] including magnesium fluoride, silicon nitride, silica, and doped silica glass[47, 70, 85]. In 2008, efficient four wave mixing (FWM) operating at low (milliwatt) continuous-wave (CW) power levels was reported in a MRR with a 575 GHz FSR spacing, in a ring resonator with a low *Q*-factor of around 60 000[39]. This was the first report of any form of nonlinear optics at milliwatt CW power levels in a silica glass-based platform. In 2010 this was followed by the first report of an integrated Kerr micro-comb[37, 38]. Another key breakthrough came in 2017[116, 117] with reports of integrated Kerr micro-combs with record small FSR's under 50 GHz. This significantly increased the available number of channels, or wavelengths, to more than 80 in the telecommunications wavelength C-band spanning 1530–1565 nm. In addition to their low FSR spacings, these Kerr micro-combs operated in a different mode to dissipative Kerr soliton (DKS) states[66–73], in a process that has been called soliton crystals[130, 131]. Many other innovative states have been reported in micro-combs, including microcombs with extremely low threshold powers[132], dark solitons[133], laser-cavity solitons[134] and others[135–140].

The devices that were used in the work reviewed here were fabricated in Hydex glass[37, 38], a CMOS compatible platform categorized as high index doped silica. Micro-ring resonators with *Q* factors ranging from 60 000 to more than 1.5 million have been achieved, with radii ranging from 592 μm down to 48 μm, corresponding to FSRs in the range 49–575 GHz. The RF signal processors used as the basis for the work reviewed here were fabricated in MRRs with FSR spacings of 200 and 49 GHz. Films of Hydex glass (n = ~1.7 at 1550 nm) were deposited via plasma-enhanced chemical vapour deposition (PECVD) and photolithographically patterned with deep ultraviolet stepper mask aligners. Waveguides with very low surface roughness were created by reactive ion etching, after which an upper cladding of silica glass (n = ~1.44 at 1550 nm) was grown. We use both lateral and vertical bus-ring coupling schemes, with a typical gap of about 200 nm. Vertical coupling can be controlled by film growth more accurately than by lithography. Hydex glass has many advantages including a very low linear loss (~ 0.06 dB·cm^{-1}), a reasonably large nonlinear parameter (0.233 W^{-1}·m^{-1}), and probably most importantly, negligible TPA even up to many gigawatts cm^{-2} of power. We achieved high *Q* factor resonators of ~1.5 million for both 49 and 200 GHz spaced MRRs. After packaging with fiber pigtails, the coupling loss can be as low as 0.5 dB per facet with the aid of on-chip mode converters.

For the 200 GHz devices, combs were generated by amplifying the CW pump power to more than 1 W (> +30 dBm). Next the wavelength was tuned from blue to red relative to the resonance wavelength, targeting a TE resonance near ~1550 nm. As the offset between the cold resonance and pump wavelength became sufficiently small, the intracavity pump power reached a threshold when modulation instability gain yielded oscillation[47], first generating primary combs with their spacing determined by the MI gain peak, which is a function of dispersion as well as the intra-cavity pump power. As the detuning changed further, microcombs with a spacing equal to the FSR appeared. While these were not soliton states, nonetheless we found that they were more than adequate for our applications to microwave signal processing. We found that it was not necessary to strictly operate in soliton states such as the dissipative Kerr solitons (DKSs)[66]. This is an important issue since, while much progress has now been made around DKS solitons[140], they nonetheless intrinsically require quite complicated pump tuning dynamics, generally employing both simultaneous amplitude (power "kicking") and wavelength sweeping, including in reverse directions, to be able to "kickstart" the solitons from chaos. Our early work on micro-combs was based on these 200 GHz FSR combs that operated in this partially coherent state. As mentioned, while not rigorous soliton states, they were still low noise enough and managed to avoid the chaotic regime[47] — we found them to be more than adequate for our RF work. They were used to successfully demonstrated many different RF signal processing functions[85, 107, 109–111].

More recently, we have used soliton crystal microcombs that featured not only this new mode of operation, but with a record low FSR spacing of 49 GHz[130, 131]. Soliton crystals arise from mode crossings and are easier and more reliable to generate than other solitons, including DKSs, and even easier than the partially coherent states of the 200 GHz resonators. They can be generated even with simple manual control of the pump wavelength and power, without any complex pump dynamics. The underlying physics for this is based on the fact that the internal optical energy in the cavity of the soliton crystals is very close to that of the chaotic state. Hence, when soliton crystals are generated from chaotic states, there is only a small net change in the intracavity optical energy. This means that there is virtually no induced shift in the resonant wavelength – either thermally or via the Kerr nonlinear effect. It is this shift in resonant wavelength and internal energy that makes DKS states so difficult to generate since the resonance "avoids" the pump wavelength via the self-induced shifting. This same effect is also responsible for greatly increasing the efficiency of the soliton crystals, so that the energy in the comb lines are much higher relative to the pump power than the DKS states, particularly for single soliton DKS states. There is one drawback of soliton crystal states, however, and that is that their spectra are not flat – they have characteristic nonuniform "curtain" patterns. While this can sometimes mean that spectral flattening is required, this is not always the case. Indeed, this issue has not prevented soliton crystals from achieving many breakthroughs in high performance photonic RF microwave functions. Even though the resonator mode-crossing, as well as anomalous dispersion, needs to be engineered, these issues have not posed a significant barrier and high fabrication yields have been achieved[64]. The specific micro-comb states reached was not important for RF applications, only that low RF noise and high coherence can be achieved, and we found this to be easy to implement with simple pump wavelength tuning. Soliton crystals have yielded the lowest noise levels of any of the micro-comb states that we have worked with and so we have focused on them for our RF work, highlighted by a low phase-noise microwave oscillator[120].

3. Photonic RF and microwave channelizers

The ability to detect and analyze RF and microwave sig-

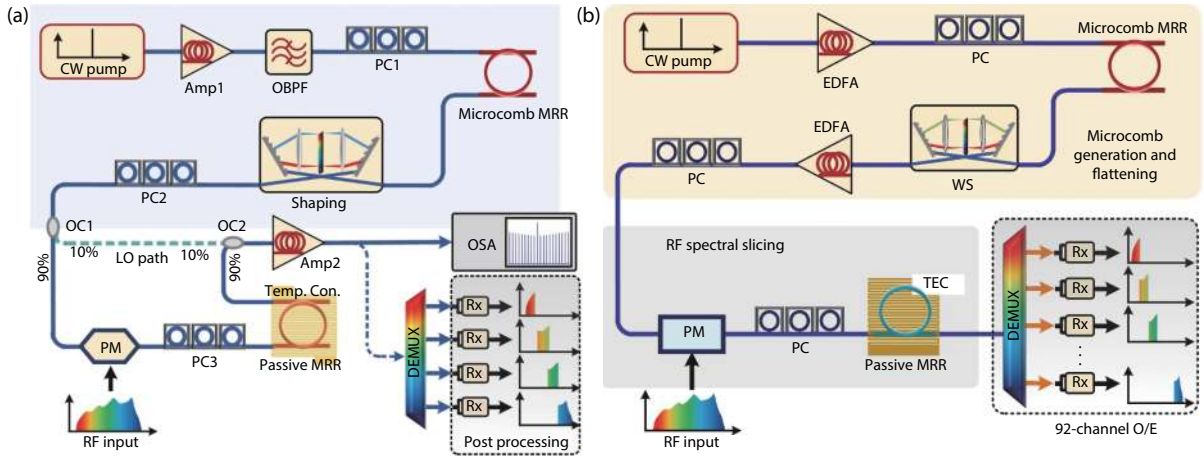

Fig. 1. (Color online) Schematic diagram of the broadband RF channelizer based on an integrated optical comb source. Amp: erbium-doped fibre amplifier. OBPF: optical bandpass filter. PC: polarization controller. MRR: micro-ring resonator. OC: optical coupler. PM: phase modulator. Temp. Con.: temperature controller. DEMUX: de-multiplexer. Rx: Receiver. OSA: optical spectrum analyzer. (a) Channelizer based on 200 GHz micro-comb MRR with 49 GHz passive MRR. (b) Schematic diagram of the broadband RF channelizer based on a soliton crystal microcomb. EDFA: erbium-doped fibre amplifier. PC: polarization controller. MRR: micro-ring resonator. WS: WaveShaper. PM: phase modulator. TEC: temperature controller. DEMUX: de-multiplexer. Rx: Receiver.

nals with very large bandwidths is critical for radar systems, electronic warfare, satellite communications and more[79, 80, 141–150]. RF and microwave channelizers, which effectively slice the RF spectrum into many frequency bands that are compatible with digital processing[149], are attractive for RF signal detection and analysis. Conventional RF channelizers usually use an array of RF filters and so are susceptible to the electronic bandwidth limitation. Photonic methods are promising for RF channelizers since they can achieve high bandwidths and also have very strong electromagnetic interference immunity.

Early reports of RF photonic channelizers used methods where RF signals were transmitted over single optical wavelengths and were then physically split to achieve spectral channelizing, usually with diffraction gratings[12], acousto-optic crystals[151], fiber Bragg gratings[152], or integrated photonic chips[153]. However, all of these methods require many narrow linewidth and spectrally dense, precisely centered, filters. Hence these systems tend to be limited in spectral resolution as well as in the number of RF channels. They also tend to have a large footprint.

Recent work on RF spectral slicing using multicasting of RF signals onto many optical wavelengths simultaneously has adopted a number of techniques including stimulated Brillouin scattering[92, 154, 155], parametric nonlinear optical processes in fiber[156, 157], spectrally incoherent sliced sources[158], discrete laser arrays[159], or electro-optic modulator generated frequency combs[149, 160, 161]. Of these, probably the most representative work[160] is where two electro-optic frequency combs were used to achieve an RF channelizer. That work used dual EO combs with slightly different FSRs and a carefully controlled offset to effectively achieve a Vernier effect to realize multi-channel detection. In contrast, the majority of approaches to channelization are essentially simply instantaneous frequency measurements designed to detect only a single narrowband signal. In Ref. [160], the RF signal was modulated on the signal comb and could thus be channelized and directly processed via analogue to digital conversion (ADC), without the need for any optical filters. The advantage of that approach, in comparison to our approach based on microcombs, is that it doesn't need a flat-top periodic optical filter. However, a significant disadvantage is that it requires a second optical frequency comb that is carefully controlled relative to the first comb, which is very challenging.

Other approaches that use wavelength scanning devices[162] or dispersive Fourier transformations[163] have also been reported, but these generally face limitations of one sort or another, including limited channel numbers and limited RF spectral resolution. They also tend to be fairly complex and expensive because of the requirement for many components such as external RF sources and mode-locked lasers etc. Integrated Kerr micro-combs[36–38, 47, 164], particularly those fabricated in CMOS compatible platforms[37–47, 49–61, 165, 166], have many advantages for broadband RF channelizers compared with discrete multi-wavelength sources, such as being able to provide a much higher number of channels or wavelengths[107–129, 167] with a greatly reduced footprint and lower complexity.

Here, we review recent work on broadband photonic RF channelizers realised through the use of integrated optical frequency Kerr microcombs, in combination with passive ring resonator filters. By using an on-chip Kerr comb source consisting of a nonlinear micro-ring resonator (MRR) with an FSR spacing of either 200 or 49 GHz, in combination with a passive on-chip MRR based filter with a FSR of 49 GHz and Q factor of 1.55×10^6, we achieved RF channelizers with high performance. The use of a 49 GHz comb resulted in a larger number of channels since the FSR of the comb source was nearly matched to the 49 GHz passive MRR. For the 200 GHz spaced comb, only every 4th resonance of the 49 GHz passive MRR could be used. We verified the RF performance experimentally at frequencies up to 26 GHz, achieving a high spectral resolution of better than 1.04 GHz for both systems. In addition to high RF performance, this approach offers a reduced footprint, lower complexity, and potentially lower cost.

4. Principle of operation

Fig. 1 shows a schematic of the RF channelizer operating by combining a microcomb as a source (in our case combs with FSRs of either 200 or 49 GHz) with a 49 GHz passive MRR that acts as a narrow optical filter. We first discuss the system based on the 200 GHz FSR microcombs, where we generated Kerr combs in the MRR by pumping with a CW tunable laser which was then amplified by an EDFA. A tunable bandpass optical filter suppressed the amplifier amplified spontaneous emission (ASE) noise and a polarization controller was then used to optimize the polarization coupled into the waveguide. When the wavelength of the pump was tuned near a resonance of the microcomb MRR, if the power was sufficiently large, then parametric gain eventually resulted in optical parametric oscillation. Finally Kerr combs with a spacing equal to the MRR FSR δ_{OFC} (~ 200 GHz) were generated. In the channelizer wavelength range the frequency of the k-th ($k = 2, 3, 4, \ldots$) comb line is

$$f_{OFC}(k) = f_{OFC}(1) + (k-1)\,\delta_{OFC}, \tag{1}$$

where $f_{OFC}(1)$ is the first comb line frequency on the red side. The microcomb lines were made uniform using a WaveShaper and then propagated through a phase modulator (PM) which multicast the RF broadband signal over all wavelengths. Finally, each of the 200 GHz comb lines, where each had the RF signal spectrum imprinted on it, were spectrally sliced, or sampled, by the second high Q MRR with a 49 GHz FSR. Hence, in the first series of experiments we had to use every 4th resonance of the passive MRR to achieve the spectral slicing, which resulted in an effective FSR with a spacing δ_{MRR} of ~196 GHz. Therefore, the RF spectrum on each of the 200 GHz microcomb lines was progressively sampled with a sequential step between resonances of about 4 GHz. The output channelized RF frequencies are:

$$\begin{aligned} f_{RF}(k) &= f_{MRR}(k) - f_{OFC}(k) \\ &= [f_{MRR}(1) - f_{OFC}(1)] + (k-1)(\delta_{MRR} - \delta_{OFC}), \end{aligned} \tag{2}$$

with $f_{RF}(k)$ being the k-th RF channelized frequency, and $f_{MRR}(k)$ the k-th center frequency of the passive MRR filter. Here, $[f_{MRR}(1) - f_{OFC}(1)]$ is the spacing between the 1st comb line and nearest filter line, which is equal to the channelized RF frequency offset, and $(\delta_{OFC} - \delta_{MRR})$ corresponds to the channelized RF frequency step between adjacent wavelengths. While the RF channels could in principle be sampled with an optical spectrum analyzer or de-multiplexer such as an AWG (arrayed waveguide grating), as long as it had a channel spacing that matched the FSR (or a multiple) of the 49 GHz MRR, in practice AWG multiplexers and similar devices generally do not have nearly as fine a resolution as the MRRs used here – they tend to have channel widths matched to the ITU grid of 50 or 100 GHz, versus the MRRs used here that had a 3 dB linewidth of about 1 GHz. The RF signals were then measured using homodyne detection, where the comb lines that had been flattened were separated first before modulating their phase, in order for them to be able to act as local oscillators (LOs). Next, they were coupled together with the channelized optical RF sidebands and then detected coherently before post processing. In the initial work based on the 200 GHz combs[113], however, we only measured the optical spectrum and not the actual RF waveform, to demonstrate the effectiveness of our method, postponing the channel demultiplexing and RF detection to our subsequent papers. Regardless, even in that initial work the large number of wavelengths generated by the micro-comb resulted in a large channel number, with very broadband RF channelizing compatible with digital channel bandwidths.

That first work was followed by an RF channelizer based on a 49 GHz microcomb combined with the 49 GHz passive MRR filter[122] that resulted in an RF photonic channelizer with significantly better performance. This was a result of the fact that the two MRRs had approximately equal FSRs, at 49 GHz. The first MRR generated a soliton crystal microcomb that the next MRR acted on as a passive filter. Using the finer spaced (than the original 200 GHz) microcomb had two main benefits. First, the fact that the FSR of the comb source was ¼ of the original work, meant that it generated as many as 92 wavelength channels across the C-band (versus 20 in the initial work). This resulted in a much larger operational bandwidth (instantaneous, without thermal tuning) of 8.08 GHz – > 22 times larger than the 200 GHz comb device[113]. Secondly, by closely matching the FSR of the second integrated high-Q MRR to the first, in order to sample the RF spectrum using the Vernier effect, a small RF channelization increment of only 87.5 MHz was realized. This effectively resulted in simultaneous and continuous (both temporally and spectrally) RF spectrum channelization, since the channel step was comparable to the passive MRR spectral resolution of 121.4 MHz. Another difference between the second device over the first one is that in the later device we used parallel phase to intensity modulation conversion (PM-IM) for all wavelength channels. This directly resulted in RF signal being generated in a very stable and compact scheme without the use of a separate local oscillator path. Finally, the operation frequency range of the channelizer could be tuned dynamically by varying the offset frequency between the passive MRR and the microcomb. Thermally tuning the passive MRR enabled us to achieve RF channelization for a very large frequency range of 17.55 GHz. In addition to yielding a very high performance in the RF domain, our approach has lower complexity, smaller footprint, and even lower cost.

The second broadband RF channelizer (Fig. 1(b)) is very similar to the previous device and also contains 3 modules. The first consists of comb generation followed by spectral flattening. Here, a MRR was driven by a CW pump to initiate parametric oscillation. The high Q factor (> 10^6) of the MRR, together with its high nonlinear FOM and anomalous dispersion, together generated sufficient parametric gain to produce Kerr soliton crystal micro-combs. The nature of the oscillation state of the microcomb was determined primarily by the pump to resonance detuning together with the pump power. By sweeping the pump wavelength from blue to red, a range of dynamic nonlinear states could be achieved, including coherent soliton states. The comb lines can also be labelled by Eqs. (1) and (2) except that now the number of lines is much larger. N microcomb lines are generated with a spacing of δ_{OFC}, the optical frequency of the k-th (k = 1, 2, 3, …, 92) comb line is given by Eq. (1). An optical WaveShaper was again used to flatten the comb line powers.

In the second module, the flattened comb lines were passed through an electrooptical phase modulator, where the input broadband RF signal was multicast onto all

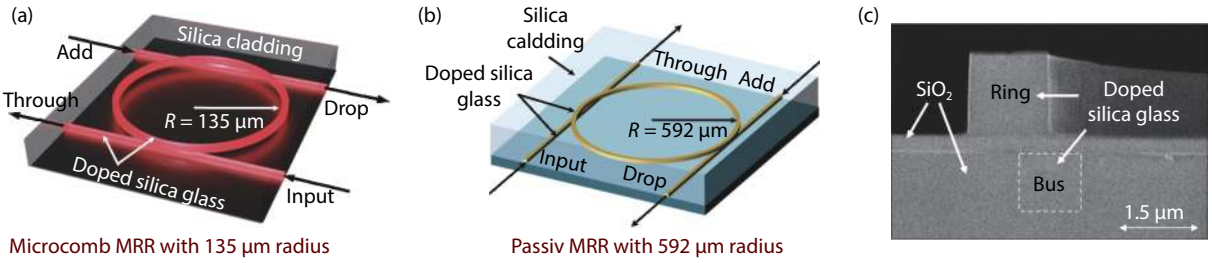

Fig. 2. (Color online) Schematic illustration of the (a) 200 GHz-FSR MRR and (b) 49 GHz-FSR MRR. (c) SEM image of the cross-section of the 200 GHz MRR before depositing the silica upper cladding.

wavelengths. Next, and as before, the replicated RF spectra were sliced by the passive MRR with an FSR of δ_{MRR}, where the slicing resolution is given by the 3 dB bandwidth of the passive resonator, about 1 GHz in our case. Hence, the RF spectral segments for all channels were essentially channelized with a RF centre frequency step given by Eq. (2).

For the 49 GHz comb based device, we used phase modulation combined with notch filtering, using the transmission through port of the second passive MRR, to convert the RF/optical signal from phase modulation to intensity modulation. Phase modulation first produced both lower and upper sidebands that had opposite phases. One of the sidebands was then rejected by the notch resonance, leaving the optical carrier to beat with the other unsuppressed sideband on photodetection. Thus, the process resulted in converting the modulation format from phase modulation to single sideband intensity modulation without a local oscillator. Hence, we effectively realized N bandpass filters in parallel, each with a spectral resolution bandwidth of Δf, which was set by the resonant linewidth of the passive MRR. The RF centre frequencies $f_{RF}(k)$ were given by the relative offset between the optical carrier frequency and the passive resonance frequencies $[f_{MRR}(k) - f_{OFC}(k)]$ (see Eq. (2)). Therefore, the input RF spectrum was channelized, or demultiplexed, into N channels located at $f_{RF}(k)$ and each having a Δf bandwidth.

As mentioned, adopting this method eliminated the requirement for a separate local oscillator path to be able to achieve homodyne coherent detection. Therefore, this approach is more stable and compact than methods that require interference paths[113]. Finally, the optical signals on the different wavelength channels were de-multiplexed and then converted into the RF domain by a photodetector array, thus producing N parallel channelized RF signals, each having a Δf spectral width, which in our case was in the operation bandwidth range of typical ADCs. Following this, the RF channelized signals were converted into digital signals using an ADC array and finally analyzed further with digital domain tools.

5. 200 GHz microcomb system

Both MRRs (Fig. 2) were based on a Hydex glass, a high-index doped silica glass platform that has CMOS compatible fabrication processes. First, high-index (n = ~1.70) Hydex glass films were deposited using PECVD, then patterned using photo-lithography and then reactive ion etched to produce waveguides that featured very low surface roughness. Finally, low index Hydex (n = ~1.44 at 1550 nm) was grown, again by PECVD, to produce the upper cladding layer. The advantages of Hydex for nonlinear optical parametric oscillators (OPOs) are very low linear propagation loss (~0.06 dB·cm^{-1}), a reasonably high optical nonlinearity (~233 W^{-1}·km^{-1}), and most importantly, essentially zero two-photon absorption even at extremely high intensities of ~25 GW·cm^{-2}[38]. The low linear loss yielded Q factors for the ring resonator that exceeded one million. A scanning electron microscope (SEM) image of the 200 GHz MRR cross section is shown in Fig. 2(c). The radii of the MRR used for the microcomb generation was 200 GHz and the passive MRR used for spectral slicing were ~135 and ~ 592 μm, corresponding to FSRs of ~1.6 nm (~200 GHz) and ~0.4 nm (~49 GHz), respectively. The device was packaged with fibre pigtails with a fibre–fibre insertion loss of ~1.5 dB for the 49 GHz MRR and ~3.5 dB for the 200 GHz MRR.

The pump laser power was boosted to 500 mW and then the wavelength tuned from blue to red in order to generate the microcombs. Initially, with the pump wavelength tuned near the MRR resonance, the primary microcombs were generated first (Fig. 3(a)), which featured idler and signal frequencies in the L and S-bands with a pump – signal spacing of 19 FSRs (3.8 THz) governed by the modulational instability gain profile. When the pump to adjacent resonance wavelength offset was tuned further, the parametric gain peaks widened, followed by the appearance of secondary comb lines with a spacing equal to the FSR, driven by cascaded FWM. The final soliton crystal Kerr combs were produced with the pump wavelength at 1548.58 nm. Figs. 3(b) and 3(c) show that the ensuing microcomb was relatively flat over the full C and L bands and was more than 200-nm wide over all S, C, L, and U bands, featuring 20 wavelengths across the C-band and more than 60 wavelengths across the combined C and L-bands. The large comb spacing translated into a large Nyquist zone, with an RF bandwidth over 100 GHz. This is very difficult to achieve with either externally-modulated comb sources or mode-locked lasers.

While the 200 GHz comb did not have a spectral profile that indicated operation in the single soliton state, this did not pose a limitation. Our theoretical analysis indicated that the Kerr comb was working in a partially coherent state that featured a stable amplitude and phase. Indeed, the spatial patterns appeared to reflect operation in soliton molecule states[130, 131, 168–170], which are low noise states, similar to cavity solitons.

Since the comb source served both as an optical carrier for RF sideband generation and as a LO for RF receiving (for the 200 GHz comb), the channelized RF optical sidebands and LOs were inherently coherent, and so rigorous phase-locked comb lines were not needed. Indeed, this is an advantage compared with RF coherent receivers[171]. Similarly, any co-

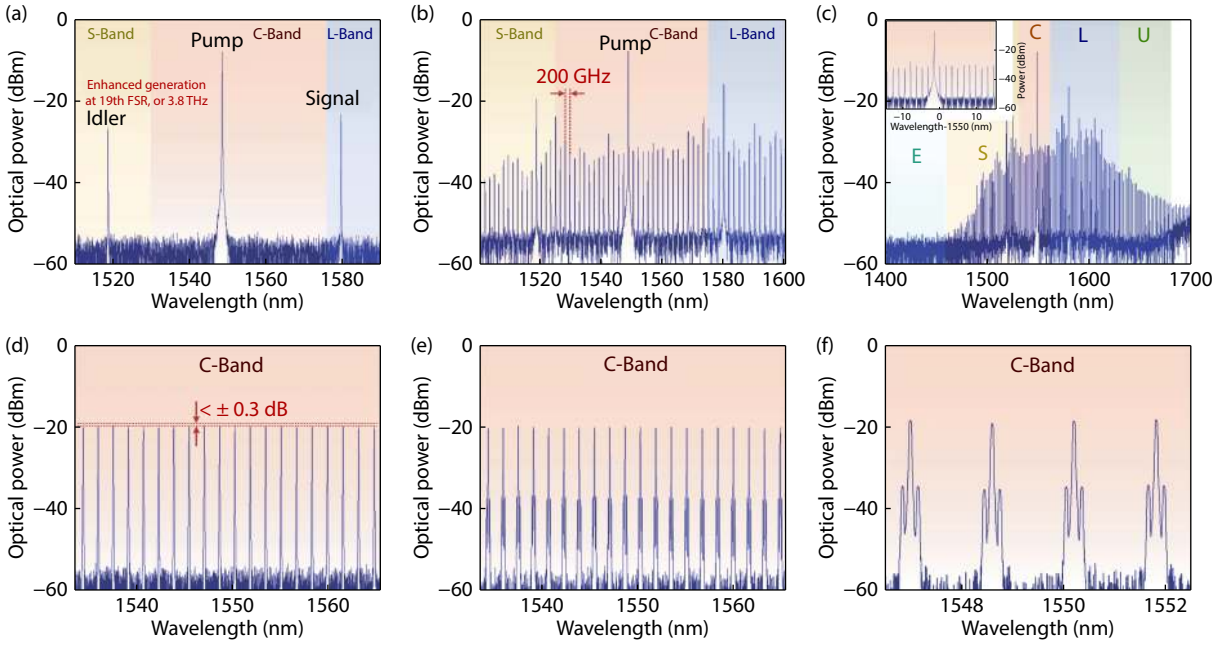

Fig. 3. (Color online) Optical spectrum for the 200 GHz FSR micro-comb device. (a) The primary comb. (b) The secondary comb. (c) The Kerr comb with 300 nm span. (d) The shaped optical comb for the channelizer with less than 0.5 dB unflatness. (e) 20 and (f) seleted 4 comb lines modulated by RF signals.

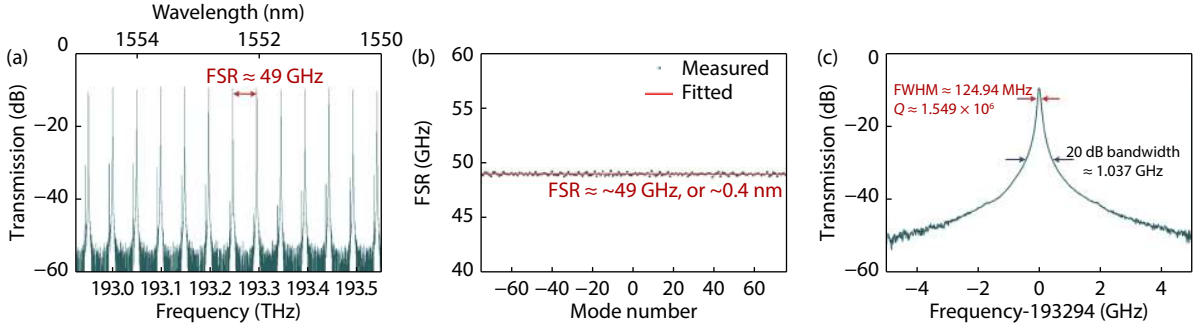

Fig. 4. (Color online) Drop-port transmission spectrum of the passive on-chip 49 GHz MRR (a) with a span of 5 nm, (b) showing an FSR of 49 GHz, and (c) a resonance at 193.294 THz with full width at half maximum (FWHM) of 124.94 MHz, corresponding to a Q factor of 1.549×10^6.

herence between adjacent wavelengths is also not needed since the wavelengths do not beat together.

The 20 C-band channels of the 200 GHz comb were shaped by a Finisar 4000S WaveShaper to equalize the power of the wavelength channels. A feedback control path accurately read and shaped the power of the comb lines as monitored by an optical spectrum analyser, which was then compared to the theoretical weights which were uniform in our case. This generated a feedback signal error to the WaveShaper so as to calibrate the system and perform accurate comb flatness and shaping to within ± 0.3 dB (Fig. 3(d)). Note that passive gain flattening filters can be used to flatten the spectrum instead of the WaveShaper. A phase modulator then multicast the RF signal onto all wavelengths, where Figs. 3(e) and 3(f) show the optical spectra of the flattened comb lines that were modulated with the RF signal. The 20 equalized channels were limited to the C-band only because of the operating wavelength range of the WS. In practice the number of wavelengths can be increased easily to 60 with the use of a C/L band WS. Next, each wavelength channel was spectrally sliced in order to extract the RF signal, by using the second MRR (49 GHz). Figs. 4(a) and 4(b) show the 49 GHz MRR drop-port transmission over a range of 5 nm, with an FSR of ~49 GHz (~0.4 nm) over 152 modes (denoting the mode at 193.294 THz as 0). The single resonance transmission (Fig. 4(c)) has a 124.94 MHz FWHM, or Q = 1.549 × 10^6, with a 1.04 GHz –20 dB bandwidth. This equals the RF resolution, which is compatible with state-of-the-art A/D[141] modules, and so our broadband RF channelizer is digital-compatible.

To demonstrate the operation principle of the RF channelizer, we show both the 200 GHz comb and the 49 GHz passive MRR transmission spectra, marking every 4th resonance that lines up with the 200 GHz comb in Fig. 5(a). We also see that for the 20 C-band comb channels, the relative offset between every 4th resonance of the 49 GHz MRR and the 200 GHz comb lines shifts linearly in the range 3.89–88.65 GHz, and this determines the RF spectral sliced frequency. This 200 GHz comb lines were measured to be at an FSR of δ_{OFC} = 200.44 GHz while four times the 49 GHz MRR lines were δ_{MRR} = 196.01 GHz. Thus the channelized RF frequency increment between channels was $\delta_{OFC} - \delta_{MRR}$ = 4.43 GHz.

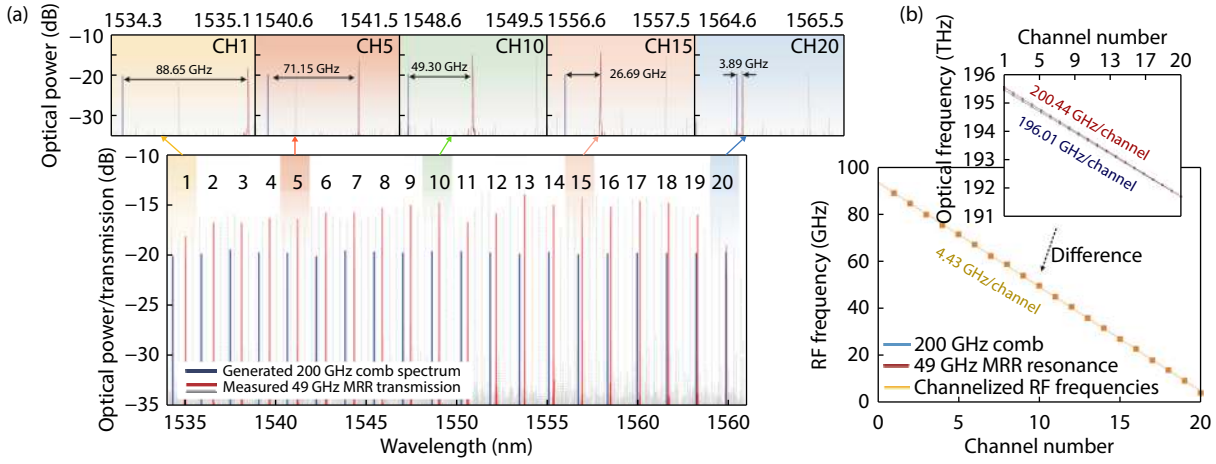

Fig. 5. (Color online) (a) The measured optical spectrum of the 200 GHz micro-comb and transmission of the 49 GHz MRR. Zoom-in views of the channels with different channelized RF frequencies. (b) Extracted channelized RF frequencies, the inset shows the corresponding optical frequencies of the comb lines and the spectral slicing resonances.

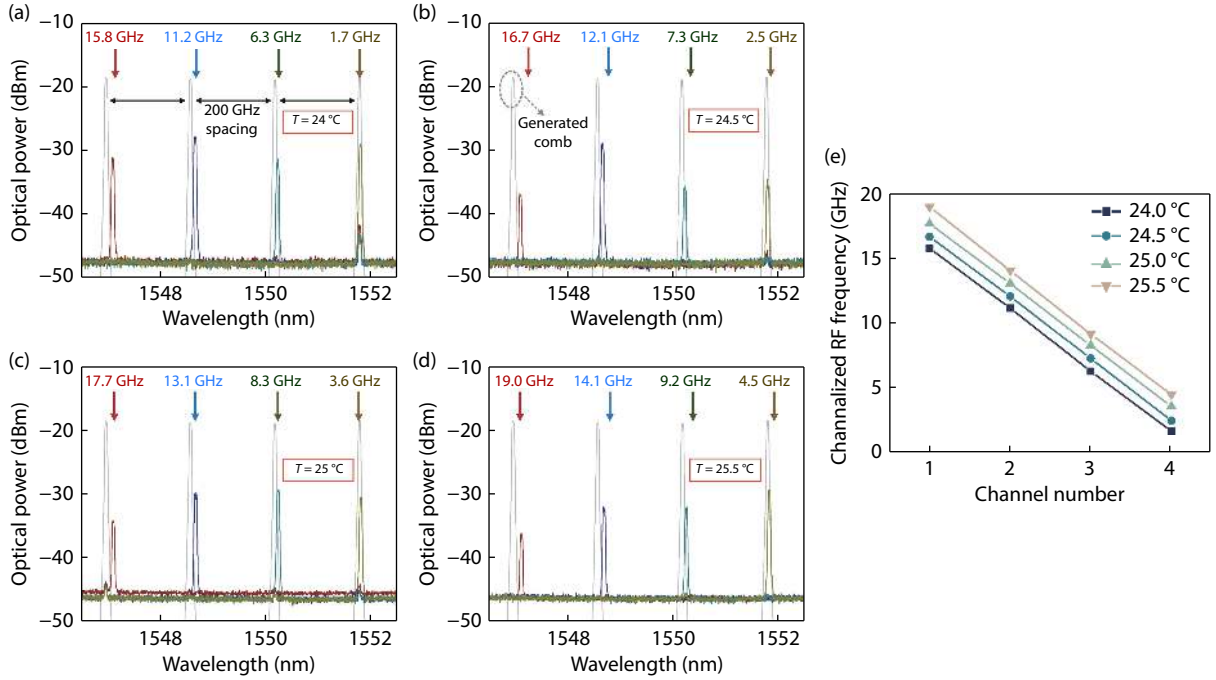

Fig. 6. RF response of the 200 GHz Channelizer. Measured optical spectrum of the 49 GHz MRR's output with different input RF frequencies, with the temperature of the 49 GHz MRR set to (a) 24.0, (b) 24.5, (c) 25.0, and (d) 25.5 °C. (e) Channelized RF frequencies at different wavelength channels with different temperatures.

We measured the frequency response of the RF channelizer up to 20 GHz. This required only 4 of 20 channels in Fig. 5, equal to 4 frequencies in the range 1.7 to 19.0 GHz. We measured the transmission of the passive 49 GHz MRR with an optical spectrum analyzer (Fig. 6), illustrating how successive RF optical sidebands featuring progressively shifting RF frequencies were channelized at different wavelengths. Optical-carrier RF tones (Fig. 6(a)) at frequencies of 1.7, 6.3, 11.2, and 15.8 GHz were contained in 4 wavelengths, yielding an RF frequency step of ~ 4.8 GHz, consistent with Fig. 5. The leaked power of channel 4 arose primarily from extraneous optical carrier tones, but these can be easily decreased by optimizing the modulation format, for example by using carrier-suppressed single sideband modulation.

In order to fully exploit the 1 GHz RF resolution of our system and fill in the gaps created by the ~ 4.8 GHz RF step size, we temperature tuned[47, 171] the passive MRR to continuously vary the relative spacing between the comb and the MRR filter wavelengths ($f_{MRR}(1) - f_{OFC}(1)$). This thermal tuning could be accomplished with a millisecond response time. Figs. 6(a)–6(d) show the output optical spectra at temperatures ranging from 24.0 to 25.5 °C. As seen in Fig. 6(e), the RF channelized frequency offset varied by ~1 GHz/°C. By combining the finer resolution of the temperature tuning with the 4.8 GHz RF step size over 60 wavelengths in the C/L-bands, this device achieved a very broad RF bandwidth > 100 GHz.

Fig. 7 shows the channelized radio frequencies of the various wavelengths extracted from Fig. 6, across the RF range 1.7–19.0 GHz, restricted only by the bandwidth of the RF modulator. Fig. 8 shows the extinction ratio of the channels

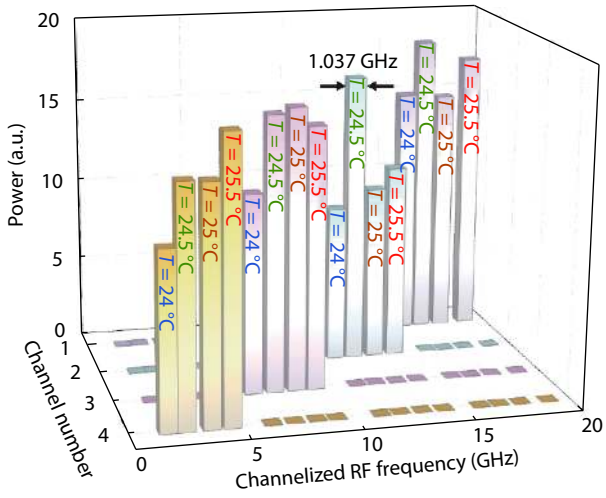

Fig. 7. (Color online) Channelized RF frequencies at different channels.

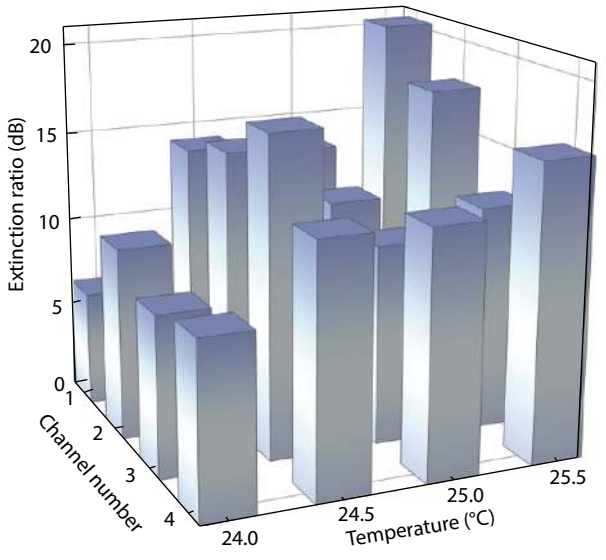

Fig. 8. (Color online) Extracted extinction ratio of channelized RF signals.

(ER - the ratio of the signal channel optical power to the maximum power of the remaining channels) deduced from Figs. 6(a)–6(d), showing an ER as high as 20 dB. The optical power non-uniformity of the channels arose predominantly from the spectral gain profile of the amplifier. This can be reduced greatly with the use of gain flattening filters. The ER was also limited by excess noise of the 2nd EDFA when adapting the optimized RF modulation format in order to increase the optical signal-to-noise-ratio (OSNR). To address this lower noise EDFAs could be used to enhance the performance. The thermal controllers had an accuracy of 0.01 °C, contributing to an error of about 50 MHz for the channelized RF frequencies, which could be reduced with more precise thermal control or through use of a feedback loop.

Although thermal tuning does not result in the channelization of the full RF spectrum simultaneously, it nevertheless allowed us to show the potential of our work. In fact, thermal tuning is not necessary, as long as the frequency increment between nearest wavelength channels (resulting from the FSR difference between the microcomb and passive MRRs) is comparable to the spectral resolution (the –20 dB linewidth of the passive MRR), which can be achieved through accurate lithographic control of the MRR FSRs. One should, for example, design δ_{OFC} = 200 GHz for the passive MRR so that δ_{MRR} = 199 GHz, still with a 1 GHz 20 dB bandwidth. Hence, the RF spectrum could be fully and simultaneously channelized and detected with a 1 GHz resolution without the use of thermal tuning. While the product of channel number and resolution – the RF bandwidth – would be a bit less than the device demonstrated here, at 60 GHz with 60 wavelengths over the C and L bands, this could be increased by using a lower FSR comb (100 GHz versus 200 GHz for example). Finally, our approach generates RF outputs by using homodyne detection. In contrast, down-conversion of the RF channelized signal would require the use of heterodyne detection with a 2nd optical comb having a specifically designed FSR and offset, which has been demonstrated by recent breakthroughs in dual-comb spectrometers[160, 172–174]. By using dual integrated microcombs with carefully designed offsets and FSRs for heterodyne detection[175–177], broadband RF signals can be channelized and then down-converted to digital bandwidths for direct A/D conversion and post processing. This approach offers a very attractive solution for photonic integrated RF receivers.

6. 49 GHz microcomb channelizer

In this section, we summarize the results for the photonic RF channelizer based on two MRRs having approximately matching FSRs at 49 GHz. This approach achieves significantly improved performance over the previous device based on a 200 GHz spaced microcomb. Here, the soliton crystal micro-comb is generated by the first MRR with a spacing equal to the FSR of 49 GHz, whereas the second MRR serves as a filter with approximately the same channel spacing. This has two main benefits. First, the smaller FSR of the soliton crystal comb source provides up to 92 wavelengths across the C-band. This results in a greatly increased instant RF bandwidth of 8.08 GHz – more than 22× that of the previous device[113]. By using high-Q integrated MRRs with approximately matching spacings to both generate the comb and filter the RF spectrum via the Vernier effect, we achieved a RF channelization step between channels of 87.5 MHz. This led to a channelization of the continuous RF spectrum since the channelization increment was less than the 121.4 MHz RF spectrum resolution. We also employed parallel phase to intensity-modulation conversion (PM-IM) over all wavelengths — which directly generated an RF output in a stable scheme and compact footprint without needing any independent local oscillator paths. Lastly, the total RF operation frequency range of the channelizer could be tuned dynamically by varying the frequency offset between the passive MRR and active microcomb. The passive MRR was thermally tuned to achieve RF channelization across a 17.55 GHz bandwidth. Apart from achieving high performance, our design yields a lower complexity, a smaller footprint, and potentially even lower cost.

Fig. 1(b) shows the setup of the broadband RF channelizer. As before, the microcomb was generated by driving the first MRR with a CW pump to induce parametric oscillation. The high 1 million Q factor of the MRR together with the high nonlinear FOM, and engineered waveguide anomalous dispersion, all contributed to achieving the parametric gain needed to produce the soliton crystal Kerr microcombs. The particular operation mode of the frequency comb was governed by the pump to resonance offset as well as the pump

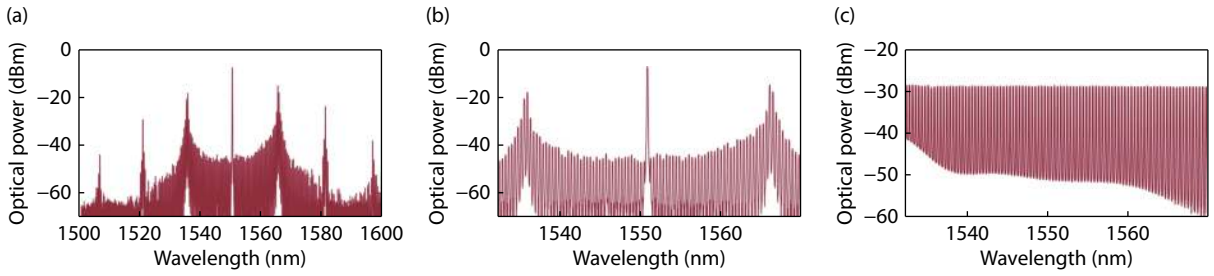

Fig. 9. (Color online) Optical spectrum of the generated soliton crystal microcomb with (a) 100 and (b) 40 nm span. (c) Flattened 92 comb lines.

power. By tuning the optical pump laser wavelength from the blue to the red, a range of dynamic nonlinear states, including coherent solitons, could be achieved. As before, for a microcomb with N wavelengths at a spacing of δ_{OFC}, the optical frequency of the k-th (k = 1, 2, 3, …, 92) comb line is given by Eq. (1). As before, a WaveShaper optical spectral shaper flattened the channel powers. For the second module, the equalized comb lines were modulated via an electro-optic phase modulator to multicast the RF signal across all wavelengths. Next, the replicated RF signals imprinted on all comb lines were sampled by the passive MRR with an FSR of δ_{MRR}, and with a resolution determined by the 3 dB resonator linewidth. As before, this resulted in a staggered RF frequency step for the RF spectral segments across the wavelength channels described by Eq. (2).

We employed notch filtering and phase modulation in this device (using the transmitted signal from the through port of the passive MRR) to perform conversion from phase to intensity modulation. First, the phase modulation produced opposite phases for the lower and upper sidebands. Next, one of the sidebands was suppressed by the filter resonance notch, leaving the other unsuppressed sideband to beat with the optical carrier upon photodetection. This essentially converted the modulation format from phase to single-sideband intensity modulation. This process therefore resulted in N bandpass filters, each with a spectral resolution of Δf determined by the passive MRR linewidth. The microwave center frequencies $f_{RF}(k)$ were given by the offset between the passive resonances and optical carriers [$f_{MRR}(k) - f_{OFC}(k)$] (Eq. (2)). Consequently, the RF input signal is demultiplexed into N segments at $f_{RF}(k)$, each with a bandwidth Δf. This method doesn't need separate physical paths for the local oscillator in order to achieve homodyne coherent detection, and therefore it is much more compact and stable than the first approach[113]. Lastly, the optical wavelengths were de-multiplexed and then changed back into the RF domain individually via an array of photodetectors, producing N channelized RF signals simultaneously, each with a Δf spectral width within the bandwidth of typical ADCs. This was then converted into digital signals with an ADCs array and processed with digital tools.

Both the passive and microcomb MRRs were fabricated in Hydex. The dispersion of the microcomb 49 GHz FSR MRR was tailored to be anomalous in the C-band to enable parametric oscillation. Further, a mode-crossing at ~1556 nm was engineered which could initiate the background wave required for soliton crystal generation. During comb generation, the pump power was boosted to ~ 2 W while the wavelength was swept manually from blue to red. As the detuning between the pump wavelength and the microcomb MRR's resonance became small enough to ensure sufficient modulation-instability gain in the microcomb MRR, primary combs were initiated. As the detuning was changed further this was followed by soliton crystal microcombs. We observed distinctive 'curtain' soliton crystal optical spectra (Figs. 9(a) and 9(b)), a resulting from the interference of the circulating tightly-packed solitons around the ring[130, 131]. The microcombs had a spacing equal to the microcomb MRR FSR of 48.9 GHz, producing up to 92 wavelength channels in the C-band. Soliton crystals are low-noise and coherent and, due to their high intracavity power, they can be easily generated just via manual tuning of the pump wavelength — much easier than DKS solitons.

Next, the power of the soliton crystal micro-comb wavelengths were equalized with a WaveShaper. The comb lines' powers were accurately shaped by using a feedback control path monitored with an optical spectral analyzer that compared the theoretical channel powers, generating an error signal that was then used to set the WaveShaper loss, with the flattened comb spectrum shown in Fig. 9(c). The 92 flattened microcomb lines were then passed through a phase modulator in order to produce optical carriers, thus multicasting the input RF signal onto all wavelengths. The passive MRR then spectrally sliced the RF replicas. We used phase modulation combined with notch filters (the passive MRR through-port transmission) to translate the passive MRR high-Q resonances into the RF domain, after which the input RF signal spectrum was channelized into N = 92 channels, each centered at $f_{RF}(k)$, and each having a bandwidth of Δf.

To quantify these experimental parameters, we measured the passive MRR transmission spectrum (Fig. 10(a)) with an incoherent broadband optical source, consisting of amplified spontaneous emission from an EDFA. Both TM and TE polarized resonances were observed, where it is seen that the channelized RF frequency $f_{RF}(k)$, calculated from the spacing between the comb line and adjacent passive resonance, successively decreases from the blue to red. The resulting RF channelized frequency (Fig. 10(b)) shows a total operation bandwidth of 8.4 and 3.8 GHz for TE and TM resonances, respectively, with a RF channelization step of 41.4 MHz (TM) and 89.5 MHz (TE) per channel. Since the channelization resolution – the linewidth of the passive resonances – was ~120 MHz, we used the TE passive resonances to obtain a larger bandwidth with lower adjacent-channel interference. By aligning the passive MRR's input light polarization to the TE mode, the TM passive resonances weren't excited and so they did not degrade the performance of the device. The dual polarization modes and birefringence of the MRRs are dis-

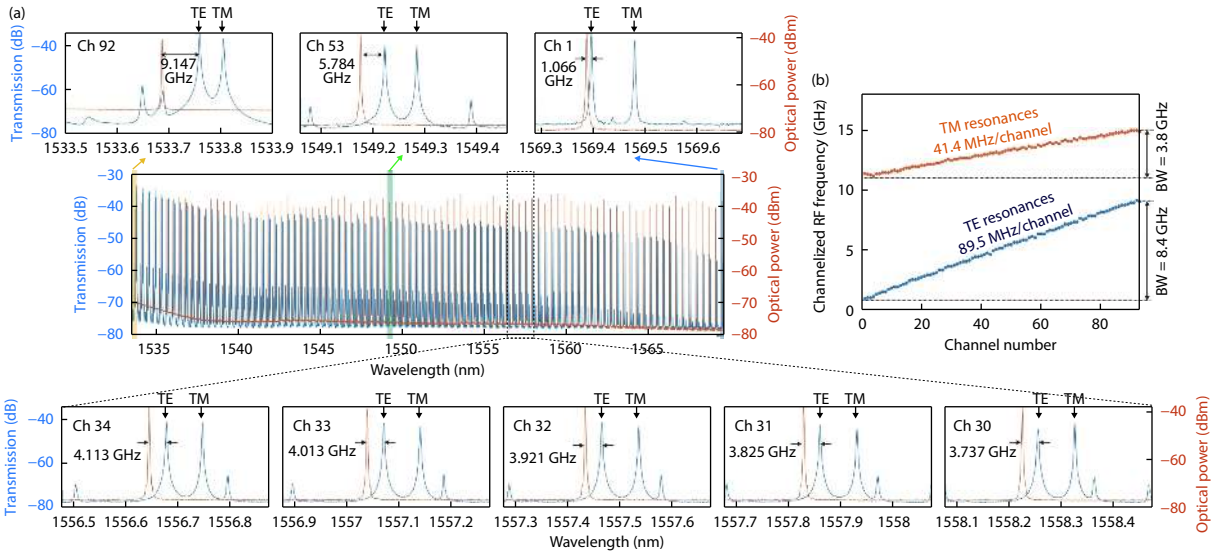

Fig. 10. (Color online) (a) The measured optical spectrum of the micro-comb and drop-port transmission of passive MRRs. (b) Extracted channelized RF frequencies of the 92 channels, calculated from the spacing between the comb lines and the passive resonances. Note that the labelled channelized RF frequencies in (a) are adopted from accurate RF domain measurements using the Vector Network Analyzer, as shown in the next figure.

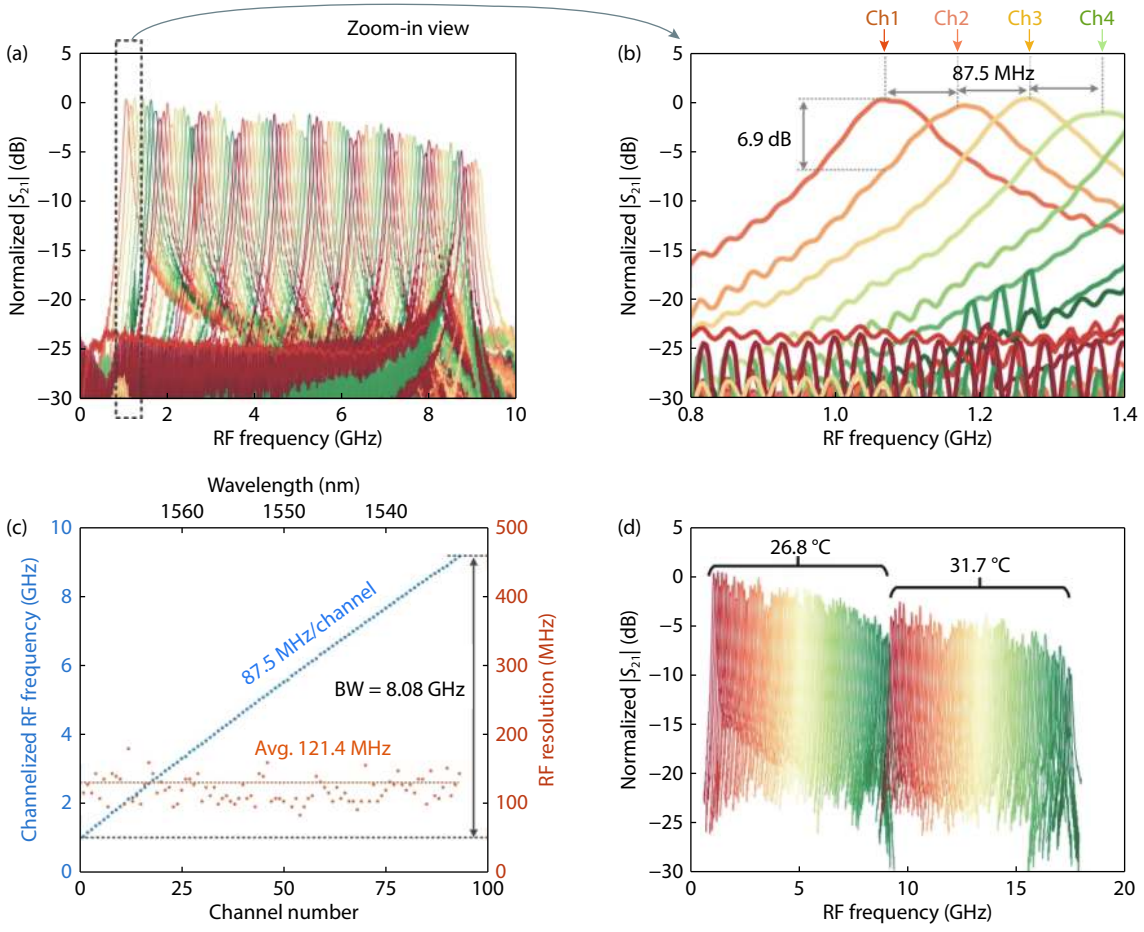

Fig. 11. (Color online) Measured RF transmission spectra of (a) the 92 channels and (b) zoom-in view of the first 4 channels. (b) Extracted channelized RF frequency and resolution. (d) Measured RF transmission spectra at different chip temperatures of the passive MRR.

cussed in another work[114, 115].

The RF spectrum was channelized into segments by the passive MRR, with each RF carried on a different wavelength, which were then de-multiplexed into spatial parallel paths and separately detected. We used a Vector RF Network Analyzer to characterize our channelizer performance. The experimental RF transmission spectra for 92 channels (Figs. 11(a) and 11(b)) verify the success of our method. Any imbalanced powers of the RF channels can be equalized by factoring the RF transmission spectra into the feedback comb shaping,

with the error signal being generated by the difference in the ideal channel weights with the RF, rather than the optical, power. The SNR of the channelizer was 23.7 dB which was extracted from the RF transmission spectra. This can be improved by increasing the extinction of the periodic optical notch filter. For the MRRs, this can be realized through adjusting the coupling coefficient from the waveguide bus to the MRR.

The RF channel centre frequencies are shown in Fig. 11(c), exhibiting a channel increment of 87.5 MHz/channel, with a total instant RF bandwidth of 8.08 GHz. This agrees with theory based on the transmission spectrum of the MRRs. The average resolution of the RF channels, derived from the RF transmission spectrum 3dB bandwidth for each channel, was 121.4 MHz. This resulted from the high Q factors of the passive MRR. This high resolution greatly relaxed the demands on the ADCs bandwidth and verifies that our approach is compatible with the relatively small bandwidths of digital components.

7. Discussion

The device based on the 49GHz soliton crystal microcomb had moderately higher adjacent-channel crosstalk. This arose mainly because of the slight difference between the RF resolution (121.4 MHz) and the channelization step (87.5 MHz). Ideally these should be equal. Nonetheless, while this situation of a channel step being less than the resolution is not perfect, any residual channel crosstalk could be eliminated by discarding redundant channels. Fine tuning the FSR of the passive MRR during fabrication would increase the RF channelization step so that it could be designed to be equal to the RF resolution. This would simultaneously result in a larger instantaneous bandwidth of 121.4 MHz × 92 = 11.17 GHz. Moreover, a much flatter passband and higher roll-off than the natural Lorentzian profile of a single MRR can be realized by using high-order optical filters[178]. Doing this would also reduce the adjacent-channel crosstalk. Finally, the filtering resolution can be increased by using higher Q factor MRRs. Finally, for our waveguide platform the dispersion was low enough that it did not affect the FSR across the wavelength range of interest, which was constant as seen in Fig. 4(a). Further, for the channelizers in general, it is only the relative FSR shift that matters and so even for larger values of dispersion, as long as the microcomb source and passive filter have similar dispersions, the RF step size will not be affected. This is verified in our case by the fact that the relative frequency shifts across the C-band that we observed were extremely linear with wavelength (Figs. 5 and 11), indicating that dispersive effects here were negligible. Of course, in cases where a completely different platform is used for the passive filter compared to the microcomb ring resonator (such as silicon-on-insulator (SOI)), then any dispersion that is large enough to affect the FSR spacing across the wavelength region would need to be accounted for and if necessary compensated for.

Lastly, by thermally tuning the passive MRR, the soliton crystal channelizer's operation bandwidth can be made tunable over a wider range. The offset between the comb and filter MRRs' resonances ($f_{MRR}(1) - f_{OFC}(1)$) can be thermally controlled on a timescale of milliseconds. As shown in Fig. 11(d), we shifted the instantaneous operating band of the channelizer from 1.006–9.147 to 9.227–17.49 GHz, continuously covering a total RF bandwidth of 16.48 GHz, by tuning the chip temperature of the passive MRR. Although thermal tuning does modify the passive MRR FSR slightly, this effect was very small. Indeed, it was a factor of ~3955 × (193.4 THz/48.9 GHz) smaller than the relative change in the offset ($f_{MRR}(1) - f_{OFC}(1)$). The change in the comb line to MRR offset (ie., $f_{MRR}(1) - f_{OFC}(1)$) resulting from thermal tuning was 8.221 GHz, while the corresponding change in the passive MRR FSR (RF channelization step) was only 2.1 MHz, and so this did not affect the device performance.

Finally, even though the RF instantaneous operation bandwidth could be moved across a wide range with thermal tuning, the RF operational lower frequency was limited to ~ 600 MHz, arising from several effects. Thermal locking of the center filter resonance to the optical carrier wavelength[39] results in a lower limit for the RF response. In addition, the intrinsically low spectral roll-off characteristic of Lorentzian lineshapes, that the passive MRRs featured here, leads to a degradation in the phase-to-intensity modulation. This can be improved by using high-order filters having steep roll-offs[178], while at the same time the thermal issues can be reduced by improving the level of control. The highest RF frequency of our channelizers was governed by the Nyquist frequency of our microcomb, which was 48.9 GHz/2 = 24.45 GHz for the soliton crystal devices and 100 GHz for the 200 GHz microcomb device. Hence, the 200 GHz system had a much higher potential maximum RF operation frequency of 100 GHz — although this involves a compromise with the number of comb lines in the useable wavelength range.

8. Conclusions

We demonstrate broadband RF channelizers based on CMOS-compatible integrated optical frequency comb sources. Broadband 200 GHz-spaced Kerr combs as well as soliton crystal combs with a 49 GHz spacing are employed. Both combs provided a record large number of wavelength channels as well as a large RF operation bandwidth. The 200 GHz comb-based device has a large potential upper bandwidth of 100 GHz, although with a limited number of channels in the C-band, typically < 20. The soliton crystal device, on the other hand, because of its lower FSR of 49 GHz that closely matched the FSRs of the MRR passive filter, yielded up to 92 wavelengths over the C-band, resulting in high performance but a correspondingly lower instantaneous RF bandwidth of 8.08 GHz. A high 121.4 MHz RF spectral resolution was realized by using a high-Q passive MRR for the optical periodic filter for both devices. For the soliton crystal device, we used phase to intensity modulation format conversion to achieve stable signal detection without any requirement for separate local oscillator paths. Dynamic adjustment of the operation RF frequency range was accomplished for both devices with the use of thermal control of the passive MRRs, achieving RF operation of up to 17.49 GHz for the soliton crystal device. This device also resulted in a broadband channelization of RF frequencies in the range 1.7–19 GHz with a high 1 GHz spectral resolution, achieved by thermal tuning of the on-chip passive MRR with a Q factor of 1.549×10^6. These micro-comb based RF channelizers are highly attractive for broadband RF channelization with large channel numbers, high resolution, compact footprint, and potentially low cost. They feature many parallel channels and are very attractive solutions for

broadband instantaneous signal detection and processing. They represent a key step towards fully integrated photonic receivers for modern RF systems.

References

[1] Radic S, Moss D, Eggleton B J. Nonlinear optics in communications: From crippling impairment to ultrafast tools. In: Optical Fiber Telecommunications V: Components and Sub-systems. Oxford, UK: Academic Press, 2008, 759

[2] Leuthold J, Koos C, Freude W. Nonlinear silicon photonics. Nat Photonics, 2010, 4, 535

[3] Li L, Patki P G, Kwon Y B, et al. All-optical regenerator of multichannel signals. Nat Commun, 2017, 8, 884

[4] Li F, Vo T D, Husko C, et al. All-optical XOR logic gate for 40Gb/s DPSK signals via FWM in a silicon nanowire. Opt Express, 2011, 19, 20364

[5] Li F, Pelusi M, Eggleton B J, et al. Error-free all-optical demultiplexing at 160Gb/s via FWM in a silicon nanowire. Opt Express, 2010, 18, 3905

[6] Ji H, Galili M, Hu H, et al. 1.28-Tb/s demultiplexing of an OTDM DPSK data signal using a silicon waveguide. IEEE Photonics Technol Lett, 2010, 22, 1762

[7] Monat C, Grillet C, Corcoran B, et al. Investigation of phase matching for third-harmonic generation in silicon slow light photonic crystal waveguides using Fourier optics. Opt Express, 2010, 18, 6831

[8] Corcoran B, Monat C, Pelusi M, et al. Optical signal processing on a silicon chip at 640Gb/s using slow-light. Opt Express, 2010, 18, 7770

[9] Ta'eed V G, Shokooh-Saremi M, Fu L B, et al. Integrated all-optical pulse regenerator in chalcogenide waveguides. Opt Lett, 2005, 30, 2900

[10] Rochette M, Kutz J N, Blows J L, et al. Bit-error-ratio improvement with 2R optical regenerators. IEEE Photonics Technol Lett, 2005, 17, 908

[11] Ferrera M, Reimer C, Pasquazi A, et al. CMOS compatible integrated all-optical radio frequency spectrum analyzer. Opt Express, 2014, 22, 21488

[12] Monat C, Grillet C, Collins M, et al. Integrated optical auto-correlator based on third-harmonic generation in a silicon photonic crystal waveguide. Nat Commun, 2014, 5, 3246

[13] Li F, Pelusi M, Xu D X, et al. All-optical wavelength conversion for 10 Gb/s DPSK signals in a silicon ring resonator. Opt Express, 2011, 19, 22410

[14] Vo T D, Corcoran B, Schroder J, et al. Silicon-chip-based real-time dispersion monitoring for 640 Gbit/s DPSK signals. J Lightwave Technol, 2011, 29, 1790

[15] Ferrera M, Park Y, Razzari L, et al. All-optical 1st and 2nd order integration on a chip. Opt Express, 2011, 19, 23153

[16] Corcoran B, Vo T D, Pelusi M D, et al. Silicon nanowire based radio-frequency spectrum analyzer. Opt Express, 2010, 18, 20190

[17] Corcoran B, Monat C, Grillet C, et al. Green light emission in silicon through slow-light enhanced third-harmonic generation in photonic-crystal waveguides. Nat Photonics, 2009, 3, 206

[18] Moss D J, van Driel H M, Sipe J E. Dispersion in the anisotropy of optical third-harmonic generation in silicon. Opt Lett, 1989, 14, 57

[19] Sipe J, Moss D, van Driel H. Phenomenological theory of optical second- and third-harmonic generation from cubic centrosymmetric crystals. Phys Rev B, 1987, 35, 1129

[20] Moss D J, Ghahramani E, Sipe J E, et al. Band-structure calculation of dispersion and anisotropy in $\chi\rightarrow(3)$ for third-harmonic generation in Si, Ge, and GaAs. Phys Rev B, 1990, 41, 1542

[21] Moss D J, van Driel H M, Sipe J E. Third harmonic generation as a structural diagnostic of ion-implanted amorphous and crystalline silicon. Appl Phys Lett, 1986, 48, 1150

[22] Moss D J, Fu L, Littler I, et al. Ultrafast all-optical modulation via two-photon absorption in silicon-on-insulator waveguides. Electron Lett, 2005, 41, 320

[23] Lamont M R E, Rochette M, Moss D J, et al. Two-photon absorption effects on self-phase-modulation-based 2R optical regeneration. IEEE Photonics Technol Lett, 2006, 18, 1185

[24] Tuniz A, Brawley G, Moss D J, et al. Two-photon absorption effects on Raman gain in single mode As_2Se_3 chalcogenide glass fiber. Opt Express, 2008, 16, 18524

[25] Pelusi M D, Luan F, Magi E, et al. High bit rate all-optical signal processing in a fiber photonic wire. Opt Express, 2008, 16, 11506

[26] Lee M W, Grillet C, Smith C L C, et al. Photosensitive post tuning of chalcogenide photonic crystal waveguides. Opt Express, 2007, 15, 1277

[27] Tomljenovic-Hanic S, Steel M J, Martijn de Sterke C, et al. High-Q cavities in photosensitive photonic crystals. Opt Lett, 2007, 32, 542

[28] Grillet C, Monat C, Smith C L, et al. Nanowire coupling to photonic crystal nanocavities for single photon sources. Opt Express, 2007, 15, 1267

[29] Ta'Eed V, Baker N J, Fu L B, et al. Ultrafast all-optical chalcogenide glass photonic circuits. Opt Express, 2007, 15, 9205

[30] Freeman D, Grillet C, Lee M W, et al. Chalcogenide glass photonic crystals. Photonics and Nanostructures-Fundamentals and Applications, 2008, 6, 3

[31] Grillet C, Freeman D, Luther-Davies B, et al. Characterization and modeling of Fano resonances in chalcogenide glass photonic crystal membranes. 2006 Conf Lasers Electro-Opt 2006 Quantum Electron Laser Sci Conf, 2006, 1

[32] Ta'Eed V G, Shokooh-Saremi M, Fu L, et al. Self-phase modulation-based integrated optical regeneration in chalcogenide waveguides. IEEE J Sel Top Quantum Electron, 2006, 12, 360

[33] Shokooh-Saremi M, Ta'Eed V G, Baker N J, et al. High-performance Bragg gratings in chalcogenide rib waveguides written with a modified Sagnac interferometer. J Opt Soc Am B, 2006, 23, 1323

[34] Lamont M R E, Ta'Eed V G, Roelens M A F, et al. Error-free wavelength conversion via cross-phase modulation in 5 cm of As_2S_3 chalcogenide glass rib waveguide. Electron Lett, 2007, 43, 945

[35] Ikeda K, Saperstein R E, Alic N, et al. Thermal and Kerr nonlinear properties of plasma-deposited silicon nitride/silicon dioxide waveguides. Opt Express, 2008, 16, 12987

[36] Levy J S, Gondarenko A, Foster M A, et al. CMOS-compatible multiple-wavelength oscillator for on-chip optical interconnects. Nat Photonics, 2010, 4, 37

[37] Razzari L, Duchesne D, Ferrera M, et al. CMOS-compatible integrated optical hyper-parametric oscillator. Nat Photonics, 2010, 4, 41

[38] Moss D J, Morandotti R, Gaeta A L, et al. New CMOS-compatible platforms based on silicon nitride and Hydex for nonlinear optics. Nat Photonics, 2013, 7, 597

[39] Ferrera M, Razzari L, Duchesne D, et al. Low-power continuous-wave nonlinear optics in doped silica glass integrated waveguide structures. Nat Photonics, 2008, 2, 737

[40] Pasquazi A, Peccianti M, Park Y, et al. Sub-picosecond phase-sensitive optical pulse characterization on a chip. Nat Photonics, 2011, 5, 618

[41] Duchesne D, Peccianti M, Lamont M R E, et al. Supercontinuum generation in a high index doped silica glass spiral waveguide. Opt Express, 2010, 18, 923

[42] Ferrera M, Park Y, Razzari L, et al. On-chip CMOS-compatible all-optical integrator. Nat Commun, 2010, 1, 29

[43] Pasquazi A, Ahmad R, Rochette M, et al. All-optical wavelength conversion in an integrated ring resonator. Opt Express, 2010, 18, 3858

[44] Pasquazi A, Park Y, Azaña J, et al. Efficient wavelength conversion and net parametric gain via four wave mixing in a high index doped silica waveguide. Opt Express, 2010, 18, 7634

[45] Peccianti M, Ferrera M, Razzari L, et al. Subpicosecond optical pulse compression via an integrated nonlinear chirper. Opt Express, 2010, 18, 7625

[46] Duchesne D, Ferrera M, Razzari L, et al. Efficient self-phase modulation in low loss, high index doped silica glass integrated waveguides. Opt Express, 2009, 17, 1865

[47] Pasquazi A, Peccianti M, Razzari L, et al. Micro-combs: A novel generation of optical sources. Phys Rep, 2018, 729, 1

[48] Del'Haye P, Schliesser A, Arcizet O, et al. Optical frequency comb generation from a monolithic microresonator. Nature, 2007, 450, 1214

[49] Peccianti M, Pasquazi A, Park Y, et al. Demonstration of an ultrafast nonlinear microcavity modelocked laser. Nat Commun, 2012, 3, 765

[50] Kues M, Reimer C, Wetzel B, et al. Passively mode-locked laser with an ultra-narrow spectral width. Nat Photonics, 2017, 11, 159

[51] Pasquazi A, Caspani L, Peccianti M, et al. Self-locked optical parametric oscillation in a CMOS compatible microring resonator: A route to robust optical frequency comb generation on a chip. Opt Express, 2013, 21, 13333

[52] Pasquazi A, Peccianti M, Little B E, et al. Stable, dual mode, high repetition rate mode-locked laser based on a microring resonator. Opt Express, 2012, 20, 27355

[53] Reimer C, Caspani L, Clerici M, et al. Integrated frequency comb source of heralded single photons. Opt Express, 2014, 22, 6535

[54] Reimer C, Kues M, Caspani L, et al. Cross-polarized photon-pair generation and bi-chromatically pumped optical parametric oscillation on a chip. Nat Commun, 2015, 6, 8236

[55] Caspani L, Reimer C, Kues M, et al. Multifrequency sources of quantum correlated photon pairs on-chip: A path toward integrated Quantum Frequency Combs. Nanophotonics, 2016, 5, 351

[56] Reimer C, Kues M, Roztocki P, et al. Generation of multiphoton entangled quantum states by means of integrated frequency combs. Science, 2016, 351, 1176

[57] Kues M, Reimer C, Roztocki P, et al. On-chip generation of high-dimensional entangled quantum states and their coherent control. Nature, 2017, 546, 622

[58] Roztocki P, Kues M, Reimer C, et al. Practical system for the generation of pulsed quantum frequency combs. Opt Express, 2017, 25, 18940

[59] Zhang Y B, Kues M, Roztocki P, et al. Induced photon correlations through the overlap of two four-wave mixing processes in integrated cavities. Laser Photonics Rev, 2020, 14, 2000128

[60] Kues M, Reimer C, Lukens J M, et al. Quantum optical microcombs. Nature Photon, 2019, 13, 170

[61] Reimer C, Sciara S, Roztocki P, et al. High-dimensional one-way quantum processing implemented on d-level cluster states. Nat Phys, 2019, 15, 148

[62] Marin-Palomo P, Kemal J N, Karpov M, et al. Microresonator-based solitons for massively parallel coherent optical communications. Nature, 2017, 546, 274

[63] Pfeifle J, Brasch V, Lauermann M, et al. Coherent terabit communications with microresonator Kerr frequency combs. Nat Photonics, 2014, 8, 375

[64] Corcoran B, Tan M X, Xu X Y, et al. Ultra-dense optical data transmission over standard fibre with a single chip source. Nat Commun, 2020, 11, 1

[65] Xu X Y, Tan M X, Corcoran B, et al. Photonic perceptron based on a kerr microcomb for high-speed, scalable, optical neural networks. Laser Photonics Rev, 2020, 14, 2000070

[66] Xu X Y, Tan M X, Corcoran B, et al. 11 TOPS photonic convolutional accelerator for optical neural networks. Nature, 2021, 589, 44

[67] Feldmann J, Youngblood N, Karpov M, et al. Parallel convolution processing using an integrated photonic tensor core. arXiv preprint arXiv: 2002.00281, 2020

[68] Spencer D T, Drake T, Briles T C, et al. An optical-frequency synthesizer using integrated photonics. Nature, 2018, 557, 81

[69] Kippenberg T J, Gaeta A L, Lipson M, et al. Dissipative Kerr solitons in optical microresonators. Science, 2018, 361, eaan8083

[70] Gaeta A L, Lipson M, Kippenberg T J. Photonic-chip-based frequency combs. Nat Photonics, 2019, 13, 158

[71] Del'Haye P, Herr T, Gavartin E, et al. Octave spanning tunable frequency comb from a microresonator. Phys Rev Lett, 2011, 107, 063901

[72] Kippenberg T J, Holzwarth R, Diddams S A. Microresonator-based optical frequency combs. Science, 2011, 332, 555

[73] Herr T, Brasch V, Jost J D, et al. Temporal solitons in optical microresonators. Nat Photonics, 2014, 8, 145

[74] Ferdous F, Miao H X, Leaird D E, et al. Spectral line-by-line pulse shaping of on-chip microresonator frequency combs. Nat Photonics, 2011, 5, 770

[75] Xue X X, Wang P H, Xuan Y, et al. Microresonator Kerr frequency combs with high conversion efficiency. Laser Photonics Rev, 2017, 11, 1600276

[76] Xue X X, Qi M H, Weiner A M. Normal-dispersion microresonator Kerr frequency combs. Nanophotonics, 2016, 5, 244

[77] Grillet C, Carletti L, Monat C, et al. Amorphous silicon nanowires combining high nonlinearity, FOM and optical stability. Opt Express, 2012, 20, 22609

[78] Choi J W, Sohn B U, Chen G F R, et al. Soliton-effect optical pulse compression in CMOS-compatible ultra-silicon-rich nitride waveguides. APL Photonics, 2019, 4, 110804

[79] Capmany J, Novak D. Microwave photonics combines two worlds. Nat Photonics, 2007, 1, 319

[80] Yao J P. Microwave photonics. J Lightwave Technol, 2009, 27, 314

[81] Marpaung D, Yao J P, Capmany J. Integrated microwave photonics. Nat Photonics, 2019, 13, 80

[82] Azaña J. Ultrafast analog all-optical signal processors based on fiber-grating devices. IEEE Photonics J, 2010, 2, 359

[83] Capmany J, Ortega B, Pastor D. A tutorial on microwave photonic filters. J Lightwave Technol, 2006, 24, 201

[84] Supradeepa V R, Long C M, Wu R, et al. Comb-based radiofrequency photonic filters with rapid tunability and high selectivity. Nat Photonics, 2012, 6, 186

[85] Wu J Y, Xu X Y, Nguyen T G, et al. RF photonics: An optical microcombs' perspective. IEEE J Sel Top Quantum Electron, 2018, 24, 1

[86] Torres-Company V, Weiner A M. Optical frequency comb technology for ultra-broadband radio-frequency photonics. Laser Photonics Rev, 2014, 8, 368

[87] Jiang Z, Huang C B, Leaird D E, et al. Optical arbitrary waveform processing of more than 100 spectral comb lines. Nat Photonics, 2007, 1, 463

[88] Liu Y, Hotten J, Choudhary A, et al. All-optimized integrated RF photonic notch filter. Opt Lett, 2017, 42, 4631

[89] Liu Y, Marpaung D, Choudhary A, et al. Link performance optimization of chip-based Si_3N_4 microwave photonic filters. J Lightwave Technol, 2018, 36, 4361

[90] Liu Y, Yu Y, Yuan S X, et al. Tunable megahertz bandwidth microwave photonic notch filter based on a silica microsphere cavity. Opt Lett, 2016, 41, 5078

[91] Marpaung D, Morrison B, Pagani M, et al. Low-power, chip-based stimulated Brillouin scattering microwave photonic filter with ultrahigh selectivity. Optica, 2015, 2, 76

[92] Choudhary A, Morrison B, Aryanfar I, et al. Advanced integrated microwave signal processing with giant on-chip Brillouin gain. J Lightwave Technol, 2017, 35, 846

[93] Marpaung D, Morrison B, Pant R, et al. Frequency agile microwave photonic notch filter with anomalously high stopband rejection. Opt Lett, 2013, 38, 4300

[94] Zhu X Q, Chen F Y, Peng H F, et al. Novel programmable microwave photonic filter with arbitrary filtering shape and linear phase. Opt Express, 2017, 25, 9232

[95] Jiang F, Yu Y, Tang H T, et al. Tunable bandpass microwave photonic filter with ultrahigh stopband attenuation and skirt selectivity. Opt Express, 2016, 24, 18655
[96] Zhu Z J, Chi H, Jin T, et al. All-positive-coefficient microwave photonic filter with rectangular response. Opt Lett, 2017, 42, 3012
[97] Yu G, Zhang W, Williams J A R. High-performance microwave transversal filter using fiber Bragg grating arrays. IEEE Photonics Technol Lett, 2000, 12, 1183
[98] Leng J S, Zhang W, Williams J A R. Optimization of superstructured fiber Bragg gratings for microwave photonic filters response. IEEE Photonics Technol Lett, 2004, 16, 1736
[99] Hunter D B, Minasian R A, Krug P A. Tunable optical transversal filter based on chirped gratings. Electron Lett, 1995, 31, 2205
[100] Hamidi E, Leaird D E, Weiner A M. Tunable programmable microwave photonic filters based on an optical frequency comb. IEEE Trans Microw Theory Tech, 2010, 58, 3269
[101] Wu R, Supradeepa V R, Long C M, et al. Generation of very flat optical frequency combs from continuous-wave lasers using cascaded intensity and phase modulators driven by tailored radio frequency waveforms. Opt Lett, 2010, 35, 3234
[102] Mansoori S, Mitchell A. RF transversal filter using an AOTF. IEEE Photonics Technol Lett, 2004, 16, 879
[103] Delgado-Pinar M, Mora J, Díez A, et al. Tunable and reconfigurable microwave filter by use of a Bragg-grating-based acousto-optic superlattice modulator. Opt Lett, 2005, 30, 8
[104] Li W, Yao J. Optical frequency comb generation based on repeated frequency shifting using two Mach-Zehnder modulators and an asymmetric Mach-Zehnder interferometer. Opt Express, 2009, 17, 23712
[105] Chen C H, He C, Zhu D, et al. Generation of a flat optical frequency comb based on a cascaded polarization modulator and phase modulator. Opt Lett, 2013, 38, 3137
[106] Saitoh T, Kourogi M, Ohtsu M. An optical frequency synthesizer using a waveguide-type optical frequency comb generator at 1.5-μm wavelength. IEEE Photonics Technol Lett, 1996, 8, 1543
[107] Nguyen T G, Shoeiby M, Chu S T, et al. Integrated frequency comb source based Hilbert transformer for wideband microwave photonic phase analysis. Opt Express, 2015, 23, 22087
[108] Xue X X, Xuan Y, Kim H J, et al. Programmable single-bandpass photonic RF filter based on kerr comb from a microring. J Lightwave Technol, 2014, 32, 3557
[109] Xu X Y, Wu J Y, Shoeiby M, et al. Reconfigurable broadband microwave photonic intensity differentiator based on an integrated optical frequency comb source. APL Photonics, 2017, 2, 096104
[110] Xu X Y, Tan M X, Wu J Y, et al. Microcomb-based photonic RF signal processing. IEEE Photonics Technol Lett, 2019, 31, 1854
[111] Xu X Y, Wu J Y, Nguyen T G, et al. Advanced RF and microwave functions based on an integrated optical frequency comb source. Opt Express, 2018, 26, 2569
[112] Xue X X, Xuan Y, Bao C Y, et al. Microcomb-based true-time-delay network for microwave beamforming with arbitrary beam pattern control. J Lightwave Technol, 2018, 36, 2312
[113] Xu X Y, Wu J Y, Nguyen T G, et al. Broadband RF channelizer based on an integrated optical frequency kerr comb source. J Lightwave Technol, 2018, 36, 4519
[114] Xu X Y, Wu J Y, Jia L N, et al. Continuously tunable orthogonally polarized RF optical single sideband generator based on microring resonators. J Opt, 2018, 20, 115701
[115] Xu X Y, Wu J Y, Tan M X, et al. Orthogonally polarized RF optical single sideband generation and dual-channel equalization based on an integrated microring resonator. J Lightwave Technol, 2018, 36, 4808
[116] Xu X Y, Wu J Y, Nguyen T G, et al. Photonic microwave true time delays for phased array antennas using a 49 GHz FSR integrated optical micro-comb source. Photon Res, 2018, 6, B30
[117] Xu X Y, Tan M X, Wu J Y, et al. Advanced adaptive photonic RF filters with 80 taps based on an integrated optical micro-comb source. J Lightwave Technol, 2019, 37, 1288
[118] Liang W, Eliyahu D, Ilchenko V S, et al. High spectral purity Kerr frequency comb radio frequency photonic oscillator. Nat Commun, 2015, 6, 7957
[119] Liu J Q, Lucas E, Raja A S, et al. Photonic microwave generation in the X- and K-band using integrated soliton microcombs. Nat Photonics, 2020, 14, 486
[120] Xu X Y, Wu J Y, Tan M X, et al. Broadband microwave frequency conversion based on an integrated optical micro-comb source. J Lightwave Technol, 2020, 38, 332
[121] Tan M X, Xu X Y, Wu J Y, et al. Photonic RF and microwave filters based on 49 GHz and 200 GHz Kerr microcombs. Opt Commun, 2020, 465, 125563
[122] Xu X Y, Tan M X, Wu J Y, et al. Broadband photonic RF channelizer with 92 channels based on a soliton crystal microcomb. J Lightwave Technol, 2020, 38, 5116
[123] Xu X, Tan M, Wu J, et al. Photonic RF and microwave integrator based on a transversal filter with soliton crystal microcombs. IEEE Trans Circuits ad Syst II, 2020, 67, 3582
[124] Xu X Y, Tan M X, Wu J, et al. Photonic RF phase-encoded signal generation with a microcomb source. J Lightwave Technol, 2020, 38, 1722
[125] Xu X Y, Tan M X, Wu J Y, et al. High performance RF filters via bandwidth scaling with Kerr micro-combs. APL Photonics, 2019, 4, 026102
[126] Tan M X, Xu X Y, Corcoran B, et al. Microwave and RF photonic fractional Hilbert transformer based on a 50 GHz Kerr microcomb. J Lightwave Technol, 2019, 37, 6097
[127] Tan M X, Xu X Y, Corcoran B, et al. RF and microwave fractional differentiator based on photonics. IEEE Trans Circuits Syst II, 2020, 67, 2767
[128] Tan M X, Xu X Y, Boes A, et al. Photonic RF arbitrary waveform generator based on a soliton crystal micro-comb source. J Lightwave Technol, 2020, 38, 6221
[129] Tan M X, Xu X Y, Wu J Y, et al. RF and microwave photonic temporal signal processing with Kerr micro-combs. Adv Phys X, 2021, 6, 1838946
[130] Cole D C, Lamb E S, Del'Haye P, et al. Soliton crystals in Kerr resonators. Nat Photonics, 2017, 11, 671
[131] Wang W Q, Lu Z Z, Zhang W F, et al. Robust soliton crystals in a thermally controlled microresonator. Opt Lett, 2018, 43, 2002
[132] Stern B, Ji X, Okawachi Y, et al. Battery-operated integrated frequency comb generator. Nature, 2018, 562, 401
[133] Xue X X, Xuan Y, Liu Y, et al. Mode-locked dark pulse Kerr combs in normal-dispersion microresonators. Nat Photonics, 2015, 9, 594
[134] Bao H L, Cooper A, Rowley M, et al. Laser cavity-soliton microcombs. Nat Photonics, 2019, 13, 384
[135] Xue X X, Zheng X P, Zhou B K. Super-efficient temporal solitons in mutually coupled optical cavities. Nat Photonics, 2019, 13, 616
[136] Zhou H, Geng Y, Cui W W, et al. Soliton bursts and deterministic dissipative Kerr soliton generation in auxiliary-assisted microcavities. Light: Sci Appl, 2019, 8, 1
[137] Bao H L, Olivieri L, Rowley M, et al. Turing patterns in a fiber laser with a nested microresonator: Robust and controllable microcomb generation. Phys Rev Res, 2020, 2, 023395
[138] di Lauro L, Li J, Moss D J, et al. Parametric control of thermal self-pulsation in micro-cavities. Opt Lett, 2017, 42, 3407
[139] Bao H L, Cooper A, Chu S T, et al. Type-II micro-comb generation in a filter-driven four wave mixing laser. Photon Res, 2018, 6, B67
[140] Shen B Q, Chang L, Liu J Q, et al. Integrated turnkey soliton microcombs. Nature, 2020, 582, 365
[141] Pan S L, Yao J P. Photonics-based broadband microwave measurement. J Lightwave Technol, 2017, 35, 3498
[142] Azana J, Madsen C, Takiguchi K, et al. Guest editorial optical sig-

nal processing. J Lightwave Technol, 2006, 24, 2484
[143] Marpaung D, Pagani M, Morrison B, et al. Nonlinear integrated microwave photonics. J Lightwave Technol, 2014, 32, 3421
[144] Minasian R A. Ultra-wideband and adaptive photonic signal processing of microwave signals. IEEE J Quantum Electron, 2016, 52, 1
[145] Zou X H, Lu B, Pan W, et al. Photonics for microwave measurements. Laser Photonics Rev, 2016, 10, 711
[146] Xu K, Wang R X, Dai Y T, et al. Microwave photonics: Radio-over-fiber links, systems, and applications. Photon Res, 2014, 2, B54
[147] Pan S L, Zhu D, Liu S F, et al. Satellite payloads pay off. IEEE Microwave, 2015, 16, 61
[148] Chen H W, Li R Y, Lei C, et al. Photonics-assisted serial channelized radio-frequency measurement system with nyquist-bandwidth detection. IEEE Photonics J, 2014, 6, 1
[149] Xie X J, Dai Y T, Ji Y, et al. Broadband photonic radio-frequency channelization based on a 39-GHz optical frequency comb. IEEE Photonics Technol Lett, 2012, 24, 661
[150] Wang W S, Davis R L, Jung T J, et al. Characterization of a coherent optical RF channelizer based on a diffraction grating. IEEE Trans Microw Theory Tech, 2001, 49, 1996
[151] Rhodes W T. Acousto-optic signal processing: Convolution and correlation. Proc IEEE, 1981, 69, 65
[152] Hunter D B, Edvell L G, Englund M A. Wideband microwave photonic channelised receiver. 2005 International Topical Meeting on Microwave Photonics, 2005, 249
[153] Winnall S T, Lindsay A C, Austin M W, et al. A microwave channelizer and spectroscope based on an integrated optical Bragg-grating Fabry-Perot and integrated hybrid Fresnel lens system. IEEE Trans Microw Theory Tech, 2006, 54, 868
[154] Xu W Y, Zhu D, Pan S L. Coherent photonic radio frequency channelization based on dual coherent optical frequency combs and stimulated Brillouin scattering. Opt Eng, 2016, 55, 046106
[155] Zou X H, Li W Z, Pan W, et al. Photonic-assisted microwave channelizer with improved channel characteristics based on spectrum-controlled stimulated Brillouin scattering. IEEE Trans Microw Theory Tech, 2013, 61, 3470
[156] Bres C S, Zlatanovic S, Wiberg A O J, et al. Parametric photonic channelized RF receiver. IEEE Photon Technol Lett, 2011, 23, 344
[157] Wiberg A O J, Esman D J, Liu L, et al. Coherent filterless wideband microwave/millimeter-wave channelizer based on broadband parametric mixers. J Lightwave Technol, 2014, 32, 3609
[158] Zou X H, Pan W, Luo B, et al. Photonic approach for multiple-frequency-component measurement using spectrally sliced incoherent source. Opt Lett, 2010, 35, 438
[159] Volkening F A. Photonic channelized RF receiver employing dense wavelength division multiplexing. U. S. Patent, 724 583 3B1, 2007
[160] Xie X J, Dai Y T, Xu K, et al. Broadband photonic RF channelization based on coherent optical frequency combs and I/Q demodulators. IEEE Photonics J, 2012, 4, 1196
[161] Li Z, Zhang X M, Chi H, et al. A reconfigurable microwave photonic channelized receiver based on dense wavelength division multiplexing using an optical comb. Opt Commun, 2012, 285, 2311
[162] Li R Y, Chen H W, Yu Y, et al. Multiple-frequency measurement based on serial photonic channelization using optical wavelength scanning. Opt Lett, 2013, 38, 4781
[163] Hao W H, Dai Y T, Yin F F, et al. Chirped-pulse-based broadband RF channelization implemented by a mode-locked laser and dispersion. Opt Lett, 2017, 42, 5234
[164] Herr T, Hartinger K, Riemensberger J, et al. Universal formation dynamics and noise of Kerr-frequency combs in microresonators. Nat Photonics, 2012, 6, 480
[165] Caspani L, Xiong C, Eggleton B, et al. On-chip sources of quantum correlated and entangled photons. Light Sci Appl, 2017, 6, e17100
[166] da Ros F, Porto da Silva E, Zibar D, et al. Wavelength conversion of QAM signals in a low loss CMOS compatible spiral waveguide. APL Photonics, 2017, 2, 046105
[167] Xue X X, Weiner A M. Microwave photonics connected with microresonator frequency combs. Front Optoelectron, 2016, 9, 238
[168] Coen S, Randle H G, Sylvestre T, et al. Modeling of octave-spanning Kerr frequency combs using a generalized mean-field Lugiato–Lefever model. Opt Lett, 2012, 38, 37
[169] Chembo Y K, Menyuk C R. Spatiotemporal Lugiato-Lefever formalism for Kerr-comb generation in whispering-gallery-mode resonators. Phys Rev A, 2013, 87, 053852
[170] Guo H, Karpov M, Lucas E, et al. Universal dynamics and deterministic switching of dissipative Kerr solitons in optical microresonators. Nat Phys, 2017, 13, 94
[171] Xue X X, Xuan Y, Wang C, et al. Thermal tuning of Kerr frequency combs in silicon nitride microring resonators. Opt Express, 2016, 24, 687
[172] Bernhardt B, Ozawa A, Jacquet P, et al. Cavity-enhanced dual-comb spectroscopy. Nat Photonics, 2010, 4, 55
[173] Ideguchi T, Poisson A, Guelachvili G, et al. Adaptive real-time dual-comb spectroscopy. Nat Commun, 2014, 5, 3375
[174] Millot G, Pitois S, Yan M, et al. Frequency-agile dual-comb spectroscopy. Nat Photonics, 2016, 10, 27
[175] Suh M G, Yang Q F, Yang K Y, et al. Microresonator soliton dual-comb spectroscopy. Science, 2016, 354, 600
[176] Pavlov N G, Lihachev G, Koptyaev S, et al. Soliton dual frequency combs in crystalline microresonators. Opt Lett, 2017, 42, 514
[177] Briles T C, Drake T E, Spencer D T, et al. Optical frequency synthesis using a dual-Kerr-microresonator frequency comb. Conference on Lasers and Electro-Optics, 2017, SW4N. 3
[178] Little B E, Chu S T, Absil P P, et al. Very high-order microring resonator filters for WDM applications. IEEE Photon Technol Lett, 2004, 16, 2263

Mengxi Tan received a B.Eng. degree from Changchun University of Science and Technology in opto-electronic information engineering in 2014 and a M.S. degree in optical engineering in 2017 from Beijing University of Aeronautics and Astronautics. She is currently working toward her Ph.D. degree in Professor Moss's group at Swinburne University of Technology, Melbourne, Australia. Her current research interests include integrated nonlinear optics, RF and microwave photonics, ultrahigh bandwidth optical communications and optical neural networks. She has a paper in Nature (2021) and Nature Communications (2020). She is a Student Member of the IEEE Photonics Society and the Optical Society of America.

David J. Moss is founding Director of the Optical Sciences Centre at Swinburne University of Technology in Melbourne, Australia. From 2016 to 2020 he was Director of the Centre for Microphotonics at Swinburne. From 2004 to 2014 he was with the University of Sydney and before that was a manager and senior scientist at JDS Uniphase in Ottawa Canada from 1998–2003. He received his PhD from the University of Toronto in Physics and BSc from the University of Waterloo. He currently has over 20 000 citations on Google Scholar with an h index of 92. He is a Fellow of the IEEE, OSA and SPIE.